

SOCO: Benchmarking Semantic Object Correspondence in Vision Foundation Models

Olaf Dünkel^{1*}, Basavaraj Sunagad^{2*}, Haoran Wang¹, David T. Hoffmann³,
Christian Theobalt¹, and Adam Kortylewski²

¹ Max Planck Institute for Informatics, Saarland Informatics Campus

² CISA Helmholtz Center for Information Security

³ University of Freiburg

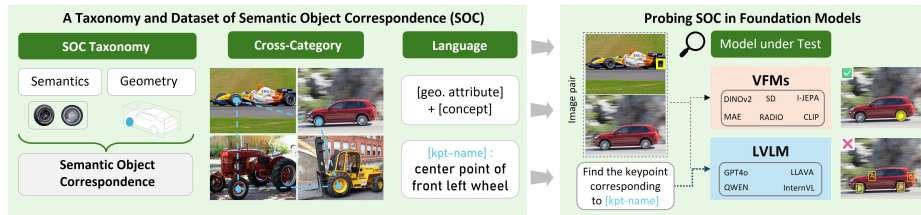


Fig. 1: SOCO provides the first taxonomy-driven, language-grounded formulation of **Semantic Object Correspondence** (SOC), enabling structured, semantically coherent, and cross-category part annotations across 100 diverse categories, which allows evaluating semantic and structured object understanding in vision foundation models (VFMs) and large vision language models (LVLMs).

Abstract. Measuring structured object understanding in vision foundation models remains challenging due to inconsistent evaluation protocols and limited part-level supervision. Semantic correspondence (SC) evaluates this capability by testing whether object parts can be matched across instances and categories under large variations in appearance, viewpoint, and geometry. To enable a systematic SC evaluation, we introduce SOCO, a new benchmark for Semantic Object Correspondence that introduces a taxonomy of correspondence types and provides consistent, functionally meaningful keypoint annotations across 100 categories and over 1M correspondence pairs. In addition, SOCO includes keypoint language descriptions, enabling the evaluation of large vision–language models (LVLMs) and their fine-grained part-level understanding. Comprehensive experiments reveal that (i) vision foundation backbones encode strong semantic structure but transfer correspondences poorly across related categories and only partially capture object-part position, (ii) LVLMs are stronger at text-prompted part localization than at visual-reference cross-image matching, exposing a gap between language-grounded localization and fine-grained visual correspondence, and (iii) correspondence performance predicts dense downstream tasks—segmentation, tracking, 3D pose estimation, and 3D detection—more strongly than ImageNet classification. Together, these findings position

* Equal contribution.

SOCO as a benchmark for structured, part-level representation quality in vision and multimodal foundation models. Dataset and code are available at <https://genintel.github.io/SOCO/>.

Keywords: Semantic Correspondence · Representation Learning · Benchmarking

1 Introduction

Visual representations form the foundation of visual intelligence. Evaluating their quality has long been central to progress in computer vision. Existing benchmarks probe distinct aspects of visual understanding, ranging from category-level recognition benchmarks such as ImageNet [16] to spatial localization tasks including detection, segmentation, and pose estimation [2, 15, 36]. However, they provide limited insight into whether a representation captures *structured object understanding*, i.e., the ability to relate semantically corresponding parts across different object instances and categories.

Recently, *semantic correspondence (SC)* has become increasingly important for evaluating self-supervised and foundation models [24, 51, 60, 66], as it measures a model’s ability to establish correspondences between object parts across different instances of a category—a capability that requires consistently capturing object structure under substantial variation in appearance, viewpoint, and geometry. The ability to establish such correspondences is crucial for transferring knowledge across related objects, for example when adapting affordances, recognition, pose estimation, or reconstruction to unseen categories, which is important for embodied and robotic systems [23, 68].

However, despite this growing adoption, progress in SC research has been constrained by the lack of a clear task definition and by the limitations of existing datasets [45, 63]. Current benchmarks conflate *two distinct abilities* in a single within-category score—recognizing the same local concept (e.g. a wheel center) and identifying its correct *repeated instance* within an object (front-left vs. rear-right wheel)—and do not evaluate transfer *across related categories* (a wheel center on a car, bus, or tractor) at all. This ambiguity limits current evaluations of modern foundation models.

We therefore propose **Semantic Object Correspondence (SOC)**, a taxonomy-driven formulation of semantic correspondence that disentangles these three abilities. SOC explicitly models the relationship between object part semantics and the overall object structure, providing a clearer separation between local concept recognition, object-relative identity, and cross-category transfer. Concretely, the taxonomy distinguishes *concept correspondence (CC)*, matching the same local concept), *semantic object correspondence (SOC)*, matching the same concept with the same object-relative identity), and *cross-category SOC* (matching object-relative keypoints across related categories through shared taxonomy concepts). This decomposition reduces annotation ambiguity, standardizes what constitutes a valid correspondence across object categories and viewpoints, and makes distinct model failure modes separately measurable.

Building on this definition, we present **SOCO**, a **Semantic Object CO**rrespondence dataset that measures SOC with taxonomy-driven keypoint annotations across *100 object categories* organized into four super-classes. Unlike prior datasets, SOCO emphasizes semantic consistency and cross-category matching, enabling structured evaluation of correspondence across varying geometry and appearance for a diverse range of man-made object and animal categories. Across a broad family of vision foundation models—including self-supervised and vision–language models such as DINO [13, 47, 60], CLIP [48], Stable Diffusion [53], and I-JEPA [3]—the decomposed evaluation reveals distinct failure modes: strong VFMs recognize local concepts but exhibit large $CC \rightarrow SOC$ drops (repeated-part confusion) and further $SOC \rightarrow Cross\text{-}SOC$ drops (limited category-level abstraction). Moreover, SOC is a practical zero-shot diagnostic of representation quality: it correlates with dense downstream tasks—segmentation, tracking, 3D pose, and 3D detection—more strongly than ImageNet classification accuracy.

As connecting vision and language modalities becomes increasingly important, benchmarks for structured object understanding should not only evaluate visual representations but also *large vision–language models (LVLMs)*. To support this, we extend SOCO with *language descriptions of correspondence keypoints*, creating a comprehensive benchmark for studying the interplay between visual correspondences and natural language in multimodal foundation models. LVLM evaluations reveal a complementary failure mode: current LVLMs are substantially stronger at text-prompted part localization within a single image than at visual-reference correspondence across images, exposing a gap between language-grounded localization and visual matching. Together, the results position SOCO as a unified benchmark for analyzing fine-grained visual reasoning and multimodal representation quality in the era of large foundation models.

In summary, our main contributions are:

- **Task formulation.** We introduce **Semantic Object Correspondence (SOC)** as a taxonomy-driven decomposition of semantic correspondence into concept correspondence, structured object understanding, and cross-category transfer.
- **Dataset.** We present **SOCO**, a large-scale benchmark built on this taxonomy, featuring 100 diverse categories, semantically grounded keypoint annotations, and over 1M correspondence pairs, with provided **language descriptions** that enable joint study of visual correspondence and language understanding in multimodal models.
- **Vision-model analysis.** Across a broad family of vision foundation models, the SOC decomposition exposes repeated-part confusion and limited cross-category abstraction even in strong dense self-supervised backbones.
- **LVLM analysis.** On the same taxonomy, current LVLMs are stronger at text-prompted part localization than at visual-reference cross-image matching, revealing a gap between language-grounded localization and fine-grained visual correspondence.

Table 1: Comparison of semantic correspondence benchmarks. SOCO uniquely combines a hierarchical keypoint taxonomy, language descriptions, and cross-category correspondence pairs while covering a large and diverse set of categories, compared to other SC datasets that include man-made objects.

Dataset	#Cats.	#Pairs	Keyp.	Taxonomy	Sep.geo.	Cross-cat.	Language
PF-WILLOW	5	900	10	✗	✗	✗	✗
PF-PASCAL	20	1.3k	4–17	✗	✗	✗	✗
SPair-71k	18	71k	3–30	✗	✗	✗	✗
DISCOBOX	12	36k	1–12	✗	✗	✓	✗
MISC210K	34	218k	5–52	✗	✗	✗	✗
SOCO	100	1M	6–32	✓	✓	✓	✓

- **SOC as a representation diagnostic.** We conduct extensive experiments across a broad family of vision models, demonstrating that SOC correlates more strongly than ImageNet k NN with dense downstream tasks, positioning SOC as a practical zero-shot diagnostic of representation quality.

2 Related work

Semantic Correspondence Benchmarks. Finding correspondences is a fundamental task in computer vision, ranging from geometric [37, 52] and stereo matching [44, 55] to optical flow [11] and tracking [71], which are typically constrained to the same instance or scene. In contrast, semantic correspondence aims to establish correspondences between object parts *across* different instances of the same category. Early datasets such as PF-PASCAL and PF-WILLOW [27], TSS [65], and Freiburg-Cars [56] defined keypoint correspondences but they were limited in scale and category diversity. Zhang et al. [79] propose a semantic correspondence benchmark based on animal keypoints from AP-10K [77]. However, it does not include man-made objects, which have more diverse keypoint types and are equally important for probing general object-level understanding. SPair-71k [45] became the de-facto standard benchmark by providing 71k image pairs across 1,800 images from 10 rigid categories of PASCAL 3D+ [73] and 8 non-rigid categories of PASCAL VOC 2012 [21], out of which 481 images are used for testing. Due to the imbalanced class selection, quadruped animals and vehicles are favored. MISC210K [63] focuses on multi-instance correspondence and increases dataset scale, but its keypoints are defined by geometric heuristics rather than a hierarchical taxonomy of semantic concepts, which—as in SPair-71k—prevents cross-category evaluation. Additionally, current SC benchmarks do not provide keypoint descriptions, preventing systematic evaluation of LVLMS. SOCO addresses these limitations by introducing the concept of *Semantic Object Correspondence*, a taxonomy-driven formulation that specifically separates geometric from non-geometric semantic correspondences and standardizes what constitutes a valid correspondence across object categories. Based on this, we create a dataset of diverse categories with taxonomy-driven SC keypoints and textual descriptions, forming the basis for a more comprehensive benchmark.

Semantic Correspondence in the Era of Foundation Models. Self-supervised and multimodal foundation models have renewed interest in semantic correspondence as a probe for representation quality [20, 60, 66], after various studies have shown that features obtained from such models can be utilized for identifying semantic correspondences in a zero-shot manner [13, 25, 40, 47, 62, 64, 80], even though they do not encode the 3D part composition particularly well [14, 19, 42, 43, 61, 67, 79]. Evaluating semantic correspondence (SC) performance provides a complementary diagnostic to conventional tasks such as classification [16, 18, 22] or segmentation [15, 81]: by measuring how well models align object parts under appearance and pose variation, it reveals whether representations encode *fine-grained part-level* and *3D-aware* structure rather than local appearance details or global category cues.

In parallel to advances in SSL, vision-language models (VLMs) such as CLIP [48], BLIP [34], and Flamingo [1] were developed to align visual and textual modalities, but their evaluation focuses mainly on retrieval and captioning [48, 57] rather than fine-grained spatial understanding. Moreover, modern large vision-language models (LVLMs) such as LLava [38], Qwen-VL [5], GPT-4V [46], and Gemini [26], extend this paradigm toward multimodal visual reasoning, yet their evaluation remains dominated by high-level tasks like VQA [39, 78] and high-level spatial reasoning [75]. BLINK [24] contains a limited number of questions targeting semantic correspondence. However, since it is built on SPair-71k and does not contain language annotations, this benchmark does not provide a comprehensive evaluation of diverse fine-grained object understanding. Our work addresses this gap by introducing a benchmark that enables a systematic evaluation of LVLMs in terms of their visual correspondence and natural language alignment, allowing analysis of how linguistic cues influence fine-grained correspondence-level understanding.

3 A Taxonomy for Semantic Correspondence

Semantic correspondence (SC) is commonly understood as the task of matching points with similar semantics across different instances of an object category. However, the definition of “semantic” correspondence has remained vague and dataset-dependent. We detail this in Sec. 3.1. To address this gap, we propose a taxonomy for the SC task, providing a principled foundation for systematic annotation and evaluation. The proposed taxonomy forms the conceptual basis for **Semantic Object Correspondence (SOC)**, a formulation that explicitly separates the local semantics and geometric position of an object part. We introduce SOC in the following section (Sec. 3.2) and show how it resolves the inconsistencies observed in existing benchmarks.

3.1 Limitations of Current SC Keypoint Annotations

Existing SC object datasets (e.g., PF-PASCAL [27], MISC210K [63], Freiburg Cars [56], SPair-71k [45]) lack a systematic, hierarchical keypoint annotation

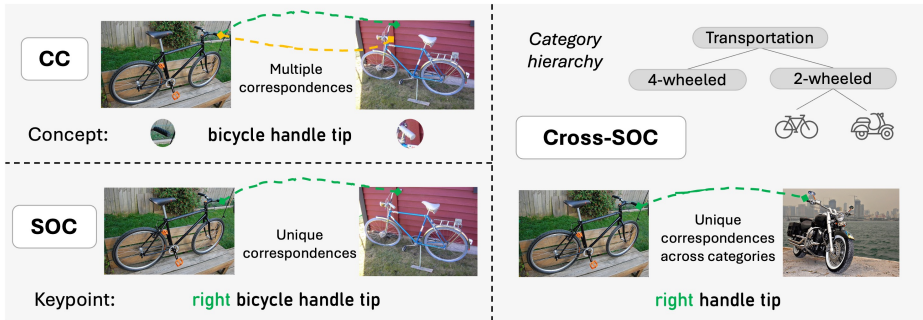


Fig. 2: Illustration of concept correspondence (CC), semantic object correspondence (SOC), and cross-category semantic object correspondence (Cross-SOC). SOC differentiates CC and SOC, which define unique correspondences by disambiguating multiple instances of the same concept via geometric attributes, such as *right*. Cross-category matches (Cross-SOC) are derived from the accompanying category hierarchy.

strategy that scales across categories. Their annotations are often defined geometrically (e.g., midpoints on TV or boat contours) rather than as self-contained semantic concepts, are ambiguous for categories with large intra-class variability (*boats*) or symmetry (*bottles*, *potted plants*), are defined on 2D projections and thus break under viewpoint change, and are sometimes internally inconsistent (e.g., the “end” of a *train*). Crucially, current benchmarks evaluate object correspondence only *within* categories, ignoring relationships between semantically related objects (cars/trucks/buses) and thereby preventing assessment of cross-category semantic transfer. We illustrate concrete cases of annotation limitations in Fig. r3 in the supplementary.

These limitations are not merely annotation artifacts but stem from the absence of a structured representation of object parts. A principled formulation requires three properties: keypoints grounded in local semantics (unambiguous identification); *identity attributes* that distinguish repeated parts (front-left vs. rear-right wheel); and an explicit hierarchical organization of semantic concepts that can be reused across categories rather than redefined per class.

3.2 A Taxonomy of Semantic Object Correspondence

To introduce a more principled formulation of semantic correspondence, we define the term **Semantic Object Correspondence (SOC)**. SOC explicitly separates two complementary aspects: the local semantics of an object part and its spatial configuration within the overall object structure. This allows probing whether a model is able to match *semantic concepts* and *semantic object keypoints* that include a positional attribute.

A **semantic concept** is defined as a uniquely identifiable location (e.g., a corner point) within an object part that is typically shared across instances of the same category. Concepts capture the local semantics of a location on an object and its immediate functional context—for instance, the *door handle* of

a car, irrespective of whether it belongs to the left or right door. In contrast, **semantic object keypoints** are concrete, instance-specific realizations of a semantic concept. Each semantic object keypoint inherits from a concept but is further disambiguated by additional positional attributes that describe its placement within the object or component, such as *left*, *right*, *bottom*, or *rear*, which are consistently defined in the object-centric coordinate system. Concepts therefore describe *what* object part is being matched, whereas semantic object keypoints specify *which instance* of that part within an object is considered. This makes finding correspondences among semantic object keypoints inherently more challenging than concept-level matching, as a model must capture or reason about both semantic identity and geometric placement within the object context to correctly identify correspondences. While matching *concepts* across two instances (*concept correspondence*, *CC*) can yield non-unique matches across keypoints, keypoint matching (*semantic object correspondence*, *SOC*) always has a unique solution. Formally, a *Semantic Object Correspondence* is defined as a match between two keypoints that share the same semantic concept and identical object-relative identity attributes, ensuring both semantic and geometric matching.

Importantly, semantic concepts are not restricted to a single category (*cross-category SOC* or *Cross-SOC*). For example, a *wheel* concept may appear in a passenger car and in a school bus or tractor. To capture this hierarchical and cross-category structure, we propose to organize all semantic concepts within a taxonomy that spans categories, super-categories, and shared concepts among objects. This hierarchy enables correspondence evaluation both within categories and across related object classes. Fig. 2 illustrates *CC*, *SOC*, and *Cross-SOC*.

Together, this formulation establishes a coherent and extensible annotation framework for semantic correspondence, which forms the conceptual foundation for the **SOCO** dataset introduced next.

4 The SOCO dataset

Building on the taxonomy introduced in Sec. 3.2, we construct **SOCO**: a large-scale, taxonomy-driven dataset for evaluating *Semantic Object Correspondence (SOC)*. SOCO is designed to address key limitations of prior correspondence benchmarks by providing (1) a standardized, semantically grounded keypoint schema, (2) cross-category and hierarchical image-keypoint pairs, (3) and a substantially broader and more balanced set of object categories. Additionally, SOCO introduces *language descriptions* for all keypoints, enabling unified evaluation of both vision and vision–language correspondence models.

4.1 Dataset Creation

In the following, we describe the steps of the dataset creation: Image collection, category distribution, keypoint annotation, and language descriptions.

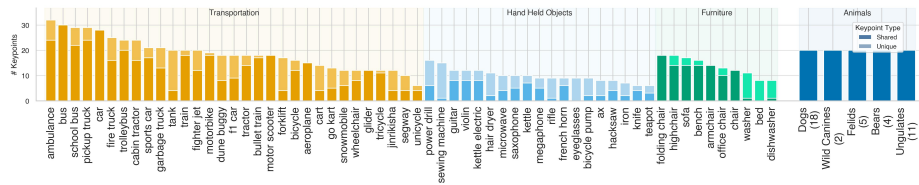


Fig. 3: Statistics of labeled keypoints. Keypoints in SOCO are annotated for a diverse set of categories from four super-categories. Each category is labeled with a subset of keypoints that are shared across multiple categories. The animal keypoints are shared across all animal categories.

Image collection. All images are samples from ImageNet. We rely on 2D and 3D annotations from ImageNet3D [41] for man-made objects and on keypoint annotations from the Animal3D dataset [74] for the animal categories. We only retain images that (1) contain valid pose metadata, (2) depict a single salient object, and (3) have a sufficiently large object size.

Category distribution. SOCO comprises **100 categories** organized into four high-level super-categories: *Transportation* (31 classes), *Hand-held Objects* (20 classes), *Furniture* (9 classes), and *Animals* (40 classes).

Keypoint annotation. All keypoints follow the introduced taxonomy. While annotations for animal categories can be acquired from animal keypoint datasets, annotations of man-made objects that follow the taxonomy do not exist and, therefore, need to be collected. For this purpose, initial annotations are acquired via Amazon Mechanical Turk and refined through a manual verification stage. A user-friendly UI with integrated keypoint reference cards was developed to enable high-quality annotations. Three qualified annotators independently complete each image annotation, and the annotations are median-aggregated after removing outliers. Every keypoint annotation is verified manually to ensure consistency and accuracy. The median per-keypoint standard deviation across annotators is 0.85% (normalized by the maximum image dimension), indicating strong agreement. During manual verification, 65.4% of annotations required only minor refinements within PCK@0.05 tolerance, while 6.8% required larger corrections, e.g., due to confused conventions (e.g. left vs. right).

Language Descriptions. Each annotated keypoint includes a human-specified language description that combines its categorical, conceptual, and geometric attributes. Descriptions are generated programmatically using the tuple (category, concept, keypoint position within the object part, object part position within the whole object), e.g., “Center point of the front left wheel of a bus”.

4.2 Dataset Statistics

Figure 3 presents the per-category keypoint distribution, including how many keypoints are shared with other categories. For each object category, 40 images are annotated, ensuring diverse viewpoints, shapes, and instance-level variations, resulting in a total of 4000 images. We construct Semantic Object Correspon-

Table 2: Model performances on SOCO. We report PCK@0.1 across concept correspondence (CC), semantic object correspondence (SOC), and its cross-category variant (Cross-SOC), as well as supercategory results. As more geometric awareness is required for SOC and more semantic abstraction for Cross-SOC, model performance drops for all models. Additional evaluations are provided in the supplementary.

Model	Accuracies by Tasks				SOC by Supercategories			
	CC	SOC	Cross-SOC	Avg	Trans.	Hand	Furn.	Animals
DINOv1	43.8	30.6 \downarrow _{13.2}	23.9 \downarrow _{19.8}	32.8	29.1	32.9	27.4	31.4
DINOv2	78.9	60.4 \downarrow _{18.5}	55.0 \downarrow _{23.9}	64.8	56.9	61.6	45.5	66.3
DINOv3	69.7	55.5 \downarrow _{14.2}	49.4 \downarrow _{20.3}	58.2	51.6	57.4	59.9	56.6
iBOT	55.2	39.6 \downarrow _{15.5}	34.1 \downarrow _{21.1}	43.0	36.1	40.1	32.8	43.9
I-JEPA	60.5	46.3 \downarrow _{14.2}	38.4 \downarrow _{22.1}	48.4	41.5	51.0	46.7	47.7
C-RADIOv3	69.0	51.1 \downarrow _{18.0}	46.3 \downarrow _{22.7}	55.5	51.7	48.1	39.7	54.8
DUNE	60.1	45.7 \downarrow _{14.4}	38.5 \downarrow _{21.6}	48.1	40.0	50.5	51.0	46.6
SD 2.1	56.0	44.8 \downarrow _{11.2}	38.3 \downarrow _{17.7}	46.4	42.4	45.3	47.7	45.6
CroCov2	15.2	10.2 \downarrow _{5.0}	7.8 \downarrow _{7.3}	11.1	11.6	12.3	10.2	8.1
MAE	14.4	9.4 \downarrow _{5.0}	7.2 \downarrow _{7.2}	10.3	10.0	11.9	11.7	7.1
PIXIO	49.5	37.5 \downarrow _{11.9}	32.9 \downarrow _{16.5}	40.0	37.3	40.2	46.7	34.2
CLIP	24.9	16.1 \downarrow _{8.9}	11.2 \downarrow _{13.7}	17.4	17.5	14.2	11.6	16.9
PE-Spatial	60.6	43.8 \downarrow _{16.8}	38.8 \downarrow _{21.9}	47.7	45.1	40.7	37.6	45.9
QWEN-L	27.2	19.4 \downarrow _{7.9}	16.2 \downarrow _{11.0}	20.9	21.7	24.1	22.6	14.5

dence (SOC) pairs by matching images within the same category, requiring at least three shared semantic keypoints. This yields around 73k SOC pairs with a total of around 560k keypoint correspondences. Concept correspondences (CC) are generated using the same pairs.

We also form cross-category (Cross-SOC) pairs, using a minimum of three shared semantic keypoints. Due to the large combinatorial space of cross-category pairings, Cross-SOC generation results in around 1.3M cross-category correspondence pairs. These complementary pairing regimes (CC, SOC, and Cross-SOC) provide progressively more challenging correspondences that support evaluation across concepts, keypoints, and different categories.

5 Experiments

In this section, we benchmark several foundation models on semantic object correspondence. We first report results for vision encoders (Sec. 5.1) and LVLMS (Sec. 5.2). Then, we analyze how SOC relates to other vision tasks (Sec. 5.3).

5.1 Vision Foundation Model Evaluation on SOCO

Evaluation Setup. In the following, we evaluate common foundation models on SOCO and compare their performance on three subtasks: **First**, *concept correspondence* (CC) evaluates whether semantic concepts can be localized correctly. **Second**, *semantic object correspondence* (SOC) evaluates whether a model also encodes the geometric position of such a semantic concept relative to the whole object. **Third**, the most challenging cross-category setting Cross-SOC probes whether representations robustly encode the evaluated concepts across different

object categories. We evaluate on three fixed random SOCO subsets, which are released together with the full dataset. For each task (CC, SOC, Cross-SOC), we use 20k pairs with a uniform number of image pairs per category, ensuring high category and image diversity while keeping a manageable evaluation cost.

We select a representative set of current representation learning approaches: Self-supervised models like the DINO family [13, 47, 60], iBOT [82], I-JEPA [3], MAE [28], and PIXIO [76], vision models trained with text supervision [7, 9, 48] and with a multi-view reconstruction objective [70], a generative image diffusion model [53, 64], and distilled models [29, 50, 54].

Following common practice in previous work [20, 60, 80], we evaluate SOC in a zero-shot manner: Given a source image I^s , a target image I^t , and a query point $p_i^s \in \mathbb{R}^2$ in the source image, the corresponding target point $p_i^t \in \mathbb{R}^2$ is computed by selecting the nearest feature vector in the target image through the argmax cosine similarity between the feature vector f_i^s at the query point and the feature map \mathcal{F}^t of the target image:

$$p_i^t = \arg \max_{q_i^t \in I^t} \text{sim}(f_i^s, \mathcal{F}^t(q_i^t)). \quad (1)$$

For model evaluation, we follow common practice [45, 79] and evaluate the matching performance via the Percentage of Correct Keypoints (PCK). It is defined by the ratio of correctly predicted keypoints that are within a radius of $R = \alpha \cdot \max(h, w)$ around the correct ground truth keypoint, where h and w refer to the height and width of the bounding box of the considered object, respectively. In the main paper, we report PCK at $\alpha = 0.1$, averaged over all image pairs of the dataset (*per-img*). Additional results are reported in the supplementary.

Experimental Results. Model evaluation results are presented in Tab. 2 and we summarize the findings below.

Strong semantic representations in vision foundation models do not imply geometric part awareness.

This finding is indicated by the consistent and substantial performance drops from CC to SOC for all evaluated models. Notably, the magnitude of this drop scales with overall model performance, suggesting that stronger semantic representations do not close the gap to geometric part awareness. This effect persists even for the best models (e.g., DINOv2): they capture semantic concepts well but struggle to disambiguate repeated object parts, as their representations do not reliably encode object-level geometry. Performance drops further in the cross-category setting Cross-SOC, as the appearance across labeled object parts changes even more strongly.

The per-supercategory columns in Tab. 2 indicate substantially different performance across categories. Further, the CC→SOC gap varies: it is largest for *Furniture* (DINOv2: SOC 45.5 vs CC 77.5) and *Transportation*, where repeated symmetric parts, such as chair/table legs and the front/rear, left/right wheels of vehicles—dominate, and smaller for the more articulated but less repetitive *Animals* and the heterogeneous *Hand-held* super-categories. Interestingly, model

rankings change with object structure: DINOv3 outperforms DINOv2 on *Furniture* (59.9 vs 45.5) despite being weaker on average, and SD 2.1 and DUNE also become comparatively stronger when repeated parts dominate. We present results for an evaluation that disentangles the geometry factor specifically (SOC-geo) in Sec. A.3, showing further ranking changes, where SD outperforms DINO models. A single average score therefore hides *which* capability a model is missing—exactly the diagnostic value our taxonomy is designed to expose.

Dense self-supervised learning objectives lead to stronger semantic correspondence representations than global alignment objectives.

Representations from the DINO model family perform particularly well for concept correspondence (CC), indicating that their self-supervised objectives learn robust local semantic features. DINOv2 shows clear gains over DINOv1, whereas DINOv3 performs slightly worse across all correspondence settings. Models such as C-RADIOv3 and DUNE, which are distilled from strong dense feature encoders including DINOv2, inherit these properties and achieve competitive performance. In contrast, models trained with global alignment objectives, such as CLIP [48], perform substantially worse, reflecting the limited spatial precision of their representations. Compared with CLIP, the larger-scale PerceptionEncoder [9] improves correspondence performance in its spatial variant, consistent with the SOCO evaluation results. Interestingly, the vision encoder of Qwen2.5-VL [7] performs similarly poorly to CLIP on this task.

Finally, reconstruction-based models such as MAE and CroCoV2 perform poorly, as their objectives primarily encourage instance-specific appearance reconstruction rather than semantic feature alignment. However, PIXIO demonstrates that scaling reconstruction-based objectives can substantially improve dense correspondence representations. I-JEPA achieves comparatively strong performance despite being trained only on ImageNet-1k.





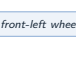





5.2 LVLM evaluation on SOC

In this section, we analyze several representative LVLMs on SOC and compare their performance in settings with and without access to textual descriptions.

Experimental Setup. Following the BLINK benchmark [24], we formulate semantic correspondence as a multiple-choice VQA task. We adopt the *CircularEval* protocol [39], where each question is presented to the LVLM four times with different permutations of the answer choices (ABCD) to enforce a consistent prediction. An answer is considered correct only if the model predicts the correct option in all four permutations, and we report accuracy under this strict criterion.

Unlike BLINK, which uses only an annotated reference image as the visual prompt, we further study how different query prompt types affect semantic correspondence performance. Specifically, we evaluate three settings: *Vis.*, *Vis.+Desc.*, and *Desc.* In all three settings, the target image with candidate keypoint markers A/B/C/D is shown to the LVLM; the settings differ only in how the query keypoint is specified (*cf.* the inset of Tab. 3). In *Vis.*, the query

Table 3: SOCO evaluation results for LVLMs. All settings show the target image with candidate keypoints; only the query differs. *Vis.* uses a marked source image, *Vis.+Desc.* additionally provides the keypoint description, and *Desc.* uses only the keypoint description as query. Gray values denote the absolute difference to *Vis.*.

Method	Vis.	Vis.+Desc.	Desc.	LVLm evaluation settings.		
<i>Baselines</i>				Setting	Query	Target
Random	0.4	0.4+0.0	0.4+0.0	Vis.		
Random++	25.0	25.0+0.0	25.0+0.0			
DINOv2	81.0	81.0+0.0	81.0+0.0			
<i>LVLms</i>				Vis.+Desc.		
LLaVA-OV-7B [33]	2.9	14.1+11.2	24.3+21.4			
InternVL3.5-8B [69]	24.9	38.5+13.6	39.6+14.7			
Qwen2.5-VL-3B [7]	5.2	17.4+12.2	29.9+24.7			
Qwen2.5-VL-7B [7]	19.4	30.8+11.4	39.1+19.7			
Qwen3-VL-4B [6]	8.6	18.0+9.4	44.4+35.8			
Qwen3-VL-8B [6]	34.2	30.8-3.4	54.0+19.8			
GPT4o [30]	30.2	30.9+0.7	37.6+7.4	Desc.		

is provided as a visual prompt, where the query keypoint is marked with visual markers in the source image. In *Vis.+Desc.*, a textual description of the query keypoint is provided additionally. In *Desc.*, the source image is omitted, and the query keypoint is specified using only the textual description; the target image and its A/B/C/D candidate markers remain visible. Because A/B/C/D are visual markers rather, a no-vision LLM cannot ground any setting and reduces to chance under CircularEval; this is matched empirically by our *Random++* baseline (25%). The gap between *Random++* and *Vis.* therefore quantifies cross-image visual matching, while *Desc.* measures text-prompted keypoint localization in the target image. Full prompts and additional illustrations are provided in the supplementary. We evaluate the LVLms on a smaller subset of SOCO with 20 image pairs per category, and adapt DINOv2 to the same 4-choice protocol by selecting the candidate patch with the highest cosine similarity to the query feature. The quantitative results on SOCO are summarized in Tab. 3. As the evaluation follows a circular protocol, the *Random++* baseline returns a random answer that is consistent across the four permuted questions of the same evaluation.

Experimental Results. LVLm evaluation results are presented in Tab. 3, and findings are discussed below.

LVLms are stronger at text-prompted keypoint localization than at visual-reference cross-image matching, exposing a gap between language-grounded localization and fine-grained visual correspondence.

A consistent trend across LVLms is that providing an explicit keypoint description (*Vis.+Desc.* and *Desc.*) improves performance compared to a purely visual query (*Vis.*). Notably, all models achieve higher accuracy in the description-only setting (*Desc.*) than in the visual-reference setting (*Vis.*). This indicates that LVLms are more effective at localizing a textually described part within a single image than at transferring a marker from a source image to the target image.

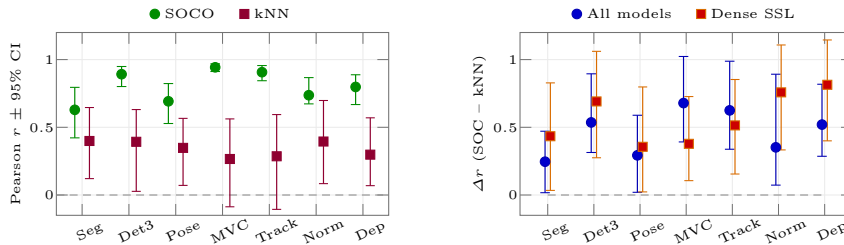


Fig. 4: Per-task Pearson r across 37 vision models, with 95% bootstrap CIs. *Left:* SOC correlates with every downstream task more strongly than ImageNet kNN. *Right:* the SOC advantage $\Delta r = r_{\text{SOC}} - r_{\text{kNN}}$ stays positive on all tasks and is preserved on a 17 subset only including models trained with dense SSL objectives.

Overall, recent models show clear improvements in both visual and language understanding. For example, the Qwen family shows consistent gains from smaller to larger models, and the Qwen3-VL-8B model outperforms its Qwen2.5-VL-7B predecessor, indicating that scaling and improved training pipelines translate into stronger semantic correspondence capabilities.

However, DINOv2 adapted to the 4-choice setting outperforms all evaluated LVLMs, achieving 81.0% compared to the best evaluated LVLm at 54.0%. This suggests that current LVLMs rely heavily on textual guidance but remain limited in their ability to align visual and textual modalities for fine-grained, cross-image correspondences. Therefore, despite recent progress, semantic correspondence on SOCO remains a challenging task for current LVLMs.

5.3 Relation to Other Vision Downstream Tasks

The previous sections evaluated SOC across a diverse set of models. In contrast, vision foundation models are typically assessed on various downstream tasks [9, 47, 50, 60, 66], spanning global objectives (e.g., image classification) and dense prediction tasks (e.g., tracking and semantic segmentation). These tasks require different evaluation protocols, such as linear probing for ImageNet [47], task-specific fine-tuning, or DPT-based training [49, 60], and their outcomes can depend strongly on hyperparameter choices.

Currently, ImageNet still remains the gold standard task for measuring representation quality [3, 47, 60], as it correlates well to other tasks [32]. However, Bolya et al. [9] have shown that capturing global representations is not necessarily aligned with strong dense semantic features.

As SOC probes dense semantic and geometric features, it is more indicative of structured visual understanding than classification-based metrics such as ImageNet kNN, while remaining practical through a simple zero-shot protocol without hyperparameter tuning. We therefore study its relation to other semantic and geometric vision tasks to assess whether it can serve as a representative diagnostic of representation quality.

Experimental Setup. We evaluate the representational quality of modern vision and vision-language backbones on a representative set of tasks using

a unified experimental protocol that builds directly on Probe3D [20]. We extend Probe3D with additional probes, including semantic object correspondence on SOCO, semantic segmentation [81], tracking [17], 3D pose estimation [41], and 3D object detection using an adapted version of the Omni3D [10] pipeline. Furthermore, we integrate a diverse set of vision foundation models, enabling performance evaluation at large scale. This unified design allows us to evaluate both fine-grained and object-level 3D understanding under identical backbone, decoding, and optimization conditions. We evaluate *depth estimation* and *surface normal prediction* on NYU [59], *geometric multi-view correspondence* on NAVI [31], *k-nearest neighbor kNN classification* on ImageNet [16], *3D pose regression* on ImageNet3D [41], *semantic segmentation* on ADE-20k [81], and *zero-shot tracking* on TAP-Vid [17], covering a wide spectrum of monocular single- and multi-view spatial reasoning requiring semantic and/or geometric understanding. We largely follow the hyperparameters used by El Banani et al. [20] and discuss implementation details in the supplementary. We open-source the evaluation framework.

Experimental Results. We compute the Pearson correlation between SOC performance and the downstream metrics across 37 vision models, with 95% bootstrap CIs (10k resamples) and leave-one-out checks. The results are summarized in Fig. 4.

SOC has a stronger correlation to various dense geometric and semantic tasks than kNN ImageNet classification.

SOC dominates kNN on every evaluated downstream task (Fig. 4), with CIs that exclude zero for the six conclusive metrics. The advantage of SOC over kNN persists after restricting the pool to 17 dense-SSL models, ruling out a dense-vs-global confound. Leave-one-out resampling agrees with the full-pool results on every metric. Overall, this suggests that SOC is a practical zero-shot diagnostic that is more aligned with dense vision tasks than ImageNet kNN.

6 Conclusion

We introduced Semantic Object Correspondence (SOC), a principled formulation of semantic correspondence that explicitly models the relationship between object parts and the overall object structure, providing a clearer separation between geometric matching and semantic object-level understanding. Building on this formulation, we developed SOCO, a large-scale benchmark that provides hierarchical part annotations, cross-category correspondences, and accompanying language descriptions, thus addressing the core limitations of existing datasets.

Through extensive evaluation of vision and multimodal foundation models, we demonstrated that SOCO exposes differences in their ability to capture fine-grained, object-centric structure. The taxonomy makes three failure modes separately measurable: the $CC \rightarrow SOC$ gap isolates repeated-part disambiguation, the $SOC \rightarrow Cross\text{-}SOC$ gap isolates category-specific concept encoding, and the $Vis.\ vs.\ Desc.$ gap in LVLMS separates cross-image visual matching

from language-grounded part localization. Our results show that: (1) models reliably match semantic concepts but struggle with object-level geometry; (2) cross-category correspondence remains challenging even for the strongest vision backbones; (3) large vision–language models are stronger at text-prompted key-point localization than at visual-reference correspondence, revealing a gap between language-grounded localization and visual matching; and (4) SOC performance correlates with dense vision tasks more strongly than ImageNet k NN, making SOC a powerful zero-shot diagnostic for representation quality.

SOCO provides a unified testbed for analyzing structured part-level visual and multimodal understanding in modern foundation models. We hope it serves as a stepping stone toward models that not only recognize objects but also understand their parts and structural relationships in a way that generalizes across categories and modalities.

Acknowledgments

AK acknowledges support via his Emmy Noether Research Group funded by the German Research Foundation (DFG) under grant number 468670075. We thank Matthis Heimberg for early analyses and experiments.

SOCO: Benchmarking Semantic Object Correspondence in Vision Foundation Models

Supplementary Material

To complement the main paper, this supplementary material provides more experimental results and implementation details.

Outline of Supplementary Material

A	More Quantitative Results on SOCO	1
A.1	Evaluation on Supercategories	1
A.2	Complementary Evaluation Protocols	2
A.3	Evaluation of Geometric Awareness (SOC-geo)	2
A.4	Evaluation for Varying PCK Thresholds	2
A.5	Analysis of Viewpoint Variation	3
A.6	Evaluation of More VFMs	3
A.7	Category-Specific Results	4
B	Example Annotations	8
B.1	Limitations of Existing SC Annotations	8
C	Evaluation Results for Other Tasks	10
C.1	Previous SC datasets	10
C.2	Other Downstream Tasks	10
D	More Details on the Performed Evaluations	11
D.1	Details on SOC Evaluation	11
D.2	Details on Evaluated Models	11
D.3	Details on Other Downstream Tasks	12
D.4	More Details of LVLm Evaluation	15
E	More Details about Annotation Pipeline	16
F	Limitations	16
G	Ethical Concerns	17

A More Quantitative Results on SOCO

This section will present additional results on the SOCO dataset: Section A.1 and Section A.4 present model evaluations on various subsets and PCK levels. Section A.6 includes an evaluation of further models in addition to the results presented in the main paper. Section A.7 reports per-category results.

A.1 Evaluation on Supercategories

Complementing the per-supercategory SOC results in the main paper (Tab. 2), Tab. r1 reports both SOC and CC for each of the four super-categories *transportation*, *hand-held*, *furniture*, and *animals*, so the CC→SOC gap per super-category can be read off directly. Interestingly, models perform worst for the furniture super-category for SOC but CC performance is even better than for the other super-categories. These larger drops might be attributed to the fact

that furniture objects have more object parts that have locally similar semantics, such as the legs of a chair. Similarly, drops are large as well for transportation categories, as they contain repeated object parts, e.g., wheels. For the SOC setting of the furniture categories, DINOv3 clearly outperforms DINOv2, indicating that DINOv3 captures geometric position better. This trend is similar for the transportation category where drops from CC to SOC are smaller for DINOv3 than for DINOv2.

A.2 Complementary Evaluation Protocols

To supplement the nearest neighbor strategy as reported in the main paper, we present more additional evaluation strategies in Tab. r2.

- 1) First, we perform an evaluation based on window softargmax [79, 80] (*soft-eval*). This consistently improves results but not by a large margin.
- 2) Second, we train a linear probe (shared across all patches) supervised and evaluated, each on 100 pairs of disjunct images (*SOC linear*). The performance improves substantially across all models. This shows that selecting a subspace of the dense features results in a learned manner leads to better matching performance, as information is discarded that changes across instances and a positional bias is added. While the best models consistently remain the best, some model rankings substantially change. For example, SD clearly improves.

A.3 Evaluation of Geometric Awareness (SOC-geo)

Relying on the explicit separation of geometric attributes and semantic concept, we further evaluate *SOC-geo*: This evaluates specifically whether a model is capable of differentiating the geometric positions of keypoints of the same concept. Given one source keypoint, the argmax is computed over all instances of the same concept for a target image of the same category. We only select image pairs where there are at least two pairs to match, which results in around 100k evaluated keypoint pairs. The random performance is 41.24% for this setting: The number of evaluated keypoints varies across categories and images. E.g., a car wheel might appear two or three times on an image but for a chair all four legs are often visible. We present the results in Tab. r2 Here, the model rankings change clearly: For example, DINOv3 outperforms DINOv2 and SD is performing best, indicating that it encodes object part position more effectively. This is in line with the analysis of the gap between SOC and CC for various supercategories.

A.4 Evaluation for Varying PCK Thresholds

Table r3 presents results for various PCK thresholds with pair averaging (*per-img*). The performances substantially drop for smaller thresholds. Interestingly, results drop less for SD than for other models.

Table r1: Model performances on SOCO across supercategories. The results are presented in the format (SOC | CC) for the four supercategories of SOCO. The model performances heavily vary for different categories and the gaps between SOC and CC change across categories and models.

Model	Transportation		Hand-held		Furniture		Animals	
DINOV1	29.09	43.00	32.92	43.16	27.41	49.47	31.45	43.30
DINOV2	56.94	76.38	61.63	74.90	45.53	77.54	66.29	83.10
DINOV3	51.61	66.14	57.39	66.28	59.86	76.24	56.57	72.49
iBOT	36.10	52.30	40.12	51.42	32.81	59.75	43.85	58.00
I-JEPA	41.48	57.13	50.96	58.21	46.71	71.71	47.74	61.40
C-RADIOv3	51.73	69.87	48.13	62.91	39.70	68.54	54.77	71.37
DUNE	39.99	55.64	50.53	59.29	51.02	71.97	46.55	61.04
SD 2.1	42.40	56.08	45.32	53.07	47.70	62.39	45.62	55.71
CroCov2	11.61	17.50	12.31	18.04	10.18	18.18	8.10	11.20
MAE	10.00	15.87	11.86	17.45	11.72	20.56	7.11	10.26
PIXIO	37.26	50.39	40.21	48.61	46.68	65.31	34.16	45.21
CLIP	17.53	27.25	14.24	22.38	11.65	25.97	16.88	24.09
PE-Spatial	45.12	62.92	40.74	53.16	37.63	61.87	45.87	62.04
QWEN-L	21.74	30.16	24.07	30.80	22.64	34.38	14.47	21.51

A.5 Analysis of Viewpoint Variation

Figure r1 presents the performance variation for varying viewpoint differences between the two matched objects. We exemplarily report the results for DINOV2, here. For this, we extract the labeled 3D pose as given by [41], compute the difference between the azimuth angles, and bin those differences. Subsequently, we compute the average performance of all matches within the considered bin. The SOC performance is lowest for a $\pi/2$ viewpoint difference, as this is the most challenging scenario, as objects are rotated by 90° and object parts are harder to disambiguate. For larger viewpoint changes, there are fewer ambiguous keypoints, increasing the performance again. For example, when two cars are observed from the left and the right side, there are not co-visible wheels that are to be matched. At the same time, CC performance remains comparably constant, indicating the pure semantic matching is still effective but geometric differentiation is limited when objects are not in the same pose.

A.6 Evaluation of More VFMs

In addition to the models presented in the main paper, we evaluate additional models on the SOCO dataset and we present the results in Table r5. We find that larger models typically outperform the base models that are evaluated in the main paper, e.g., the large variants of DINOV2, DINOV3, or C-RADIO v4. DINOV2, DINOV3, and C-RADIOv4 reach comparable performance on SOC. Additional results including the current SOTA-models on SPair-71k are presented

Table r2: SOCO results with various evaluation protocols. We report evaluation with window soft argmax (*soft-eval*), trained with a linear probe, and when only evaluating the capability of capturing the correct geometric attribute for keypoints of the same semantic concept (*SOC-geo*).

Model	SOC soft-eval	SOC linear	SOC-geo
DINOv1	32.29	34.95	56.46
DINOv2	62.71	63.26	60.97
DINOv3	55.75	60.76	66.36
iBOT	41.40	43.12	58.39
I-JEPA	47.73	44.00	61.09
C-RADIOv3	52.40	54.74	57.32
DUNE	47.11	52.62	62.48
SD 2.1	38.47	46.07	66.96
CroCov2	10.15	19.68	54.96
MAE	9.09	22.24	54.04
PIXIO	35.67	53.67	61.06
CLIP	16.84	27.61	51.45
PE-Spatial	45.76	46.61	56.72
QWEN-L	19.82	18.48	55.34

in Table r4, following the implementation of CleanDIFT [62] and GeoAware-SC [79]. Here, we also evaluate SOC for weakly-supervised models: DIY-SC [19] and SD+DINO [79] with CLIP embeddings fine-tuned on panoptic segmentation. Furthermore, we also evaluate the supervised variant of [79] relying on SD+DINO features and only relying on DINO features. We train both from scratch on SPair-71k. While weak supervision specifically used to improve semantic correspondence improves performance on this dataset as well, the performance of the models trained supervised on SPair-71k clearly drops compared to the SPair-71k test dataset performance that is substantially larger than 80%. This indicates that SOCO captures new categories that are different to the SPair-71k categories. Particularly, while animal, transportation, and furniture categories clearly improve compared to the zero-shot approach with SD+DINO features, the matching performance drops by 8.61 points for hand-held objects.

A.7 Category-Specific Results

Table r6 presents per-category results for DINOv2-B at varying PCK thresholds. The gaps between SOC and CC largely depend on the considered category. Similarly, reducing the threshold for the PCK calculation has a varying effect on different categories.

Table r3: Model performances on SOCO across multiple thresholds. The results are presented in the format (SOC | CC) for both pair averaging and per-keypoint reduction.

Model	Pair Averaging						Per Keypoint					
	PCK@0.10		PCK@0.05		PCK@0.02		PCK@0.10		PCK@0.05		PCK@0.02	
DINOV1	30.59	43.79	15.97	23.99	4.65	6.99	32.07	44.82	16.89	24.77	4.93	7.25
DINOV2	60.43	78.90	41.64	57.22	15.44	21.52	61.72	79.62	43.02	58.24	16.15	22.03
DINOV3	55.52	69.72	36.32	47.16	12.19	15.72	57.79	70.42	38.28	48.02	12.98	16.08
iBOT	39.64	55.16	21.03	30.87	5.84	8.59	41.39	56.32	22.19	31.78	6.22	8.89
C-RADIOv3	51.06	69.01	31.37	44.55	9.78	13.93	52.37	70.01	32.57	45.62	10.24	14.33
DUNE	45.72	60.12	30.19	41.36	11.09	15.20	48.02	61.05	32.03	42.26	11.89	15.66
SD 2.1	44.77	55.99	32.16	40.71	12.30	15.35	47.42	56.79	34.47	41.51	13.36	15.74
CroCov2	10.20	15.15	4.81	7.25	1.40	2.03	10.88	15.39	5.19	7.42	1.52	2.10
MAE	9.37	14.40	3.91	6.04	1.03	1.50	10.01	14.70	4.25	6.22	1.13	1.56
PIXIO	37.53	49.47	20.50	28.23	5.99	8.27	39.85	50.46	21.98	28.89	6.48	8.49
CLIP	16.06	24.93	7.08	11.49	1.76	2.81	16.85	25.68	7.51	11.92	1.90	2.95
PE-Spatial	43.84	60.61	28.16	41.00	9.52	13.97	45.09	61.49	29.28	41.87	9.99	14.28
QWEN-L	19.36	27.24	9.15	13.26	1.83	2.68	20.88	27.90	9.94	13.65	2.01	2.77

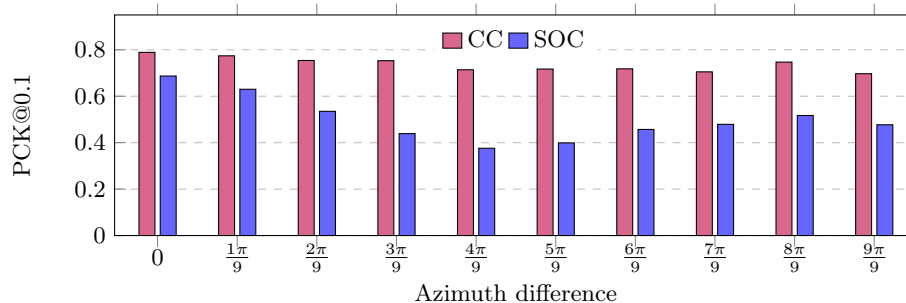


Fig. r1: PCK of DINOv2/b for increasing azimuth variation between two images, averaged over all categories. While the concept correspondence (CC) remains stable for larger viewpoint changes, SOC performance drops with a minimum for a relative orientation of objects of $\pi/2$.

Table r4: Evaluation of additional models on SOCO following the implementation of GeoAware-SC and CleanDIFT [19,43,62,79]. Results are reported for PCK@0.1 (*per-img*).

Model	SOC
SD (ft. for pan. seg., Geo-SC)	47.7
SD + DINO (SD ft pan. seg., Geo-SC)	62.9
CleanDIFT + DINO	63.4
DIY-SC (weakl. sup.)	69.2
TLR (w SD+DINO) (sup. SPair-71k)	72.9
TLR (w DINO) (sup. SPair-71k)	72.7

Table r5: Model performances on SOCO across concept correspondence (CC), semantic object correspondence (SOC) and its cross-category variants (Cross-SOC). This table extends the table presented in the main paper with additional models.

Model	CC	SOC	Cross-SOC
c_radio_3_b	69.01	51.06	46.33
clip_b16	24.93	16.06	11.22
clip_b16_laion	24.91	15.69	11.04
clip_l14	37.37	25.23	18.24
croco	15.15	10.20	7.82
dift	55.99	44.77	38.29
dino_b16	43.79	30.59	23.95
dino_s16	43.13	29.97	23.16
dinov2_b14	78.90	60.43	54.98
dinov2_b14_reg	76.31	58.03	50.87
dinov2_l14	80.68	62.40	56.94
dinov2_s14	73.99	56.67	50.25
dinov3_vitb16	69.72	55.52	49.43
dinov3_vitl16	76.56	61.36	56.15
dinov3_vits16plus	69.28	55.20	49.37
dune_vitb14	60.12	45.72	38.53
dune_vits14	50.71	38.15	31.56
ibot_b16	55.16	39.64	34.09
ibot_b16_in22k	53.07	38.39	32.87
ibot_l16	64.14	47.43	42.75
ibot_l16_in22k	66.55	49.39	44.77
ibot_s16	48.24	33.75	27.93
ijepa	60.50	46.31	38.36
mae_b16	14.40	9.37	7.15
metaclip2_vitb16	30.41	19.63	14.72
metaclip2_vitl14	38.54	25.88	18.57
metaclip2_vits16	23.26	14.81	11.32
openclip_vitb16_datacomp	34.05	22.49	16.11
openclip_vitl14_datacomp	46.02	31.79	24.52
openclip_vitl14_laion2b	33.44	22.32	15.87
perception	60.61	43.84	38.76
pixio_vitb16	49.47	37.53	32.93
pixio_vitl16	51.26	38.59	32.86
qwen_vl	27.24	19.36	16.25
radio	72.53	55.54	51.32
sam_base	35.21	25.52	20.40
siglip_b16	14.10	8.83	7.00
siglip_l16	14.53	9.60	7.47
vjepa2_1_base	60.37	44.46	38.56
vjepa2_1_large	69.69	53.21	48.10

Table r6: SOCO per-category results evaluated with DINOv2-B across multiple thresholds (pair averaging).

Category	PCK@0.10		PCK@0.05		PCK@0.02	
	CC	SOC	CC	SOC	CC	SOC
aeroplane	83.4	72.9	69.7	59.1	34.2	28.4
ambulance	87.7	54.1	74.0	43.6	36.4	20.8
american black bear	72.7	54.1	44.2	32.3	12.7	8.8
arctic fox	81.9	65.4	56.8	44.0	17.3	13.1
armchair	79.2	48.7	57.7	36.0	21.0	13.1
ax	81.2	55.5	60.7	35.4	27.1	16.5
bed	74.8	40.4	63.7	34.5	32.4	17.6
bench	79.1	37.0	59.0	27.5	22.5	9.5
bicycle	85.7	83.8	65.7	64.7	26.1	25.6
bicycle pump	89.7	69.1	80.9	57.1	43.0	28.5
bighorn	85.1	67.6	55.6	40.7	15.4	12.5
boston bull	87.8	59.5	62.9	40.5	19.9	13.0
brittany spaniel	89.4	74.3	62.1	50.1	21.2	17.2
brown bear	75.7	61.2	47.1	36.5	14.6	11.2
bullet train	62.4	48.7	38.3	28.8	11.6	8.5
bus	82.6	54.4	68.0	43.9	29.8	18.4
cabin tractor	72.8	54.9	48.4	34.7	11.5	8.1
cairn	78.6	62.5	55.7	40.4	20.1	13.7
car	90.1	62.1	78.5	54.2	36.0	26.2
cart	53.8	40.8	36.6	26.6	14.0	9.4
chair	85.0	42.0	69.5	33.3	31.9	14.7
cheetah	89.5	78.0	70.6	59.5	27.8	24.5
chow	90.1	64.1	65.7	45.1	23.7	16.5
cougar	85.6	64.1	60.8	42.2	21.3	15.4
dishwasher	68.4	43.0	48.3	29.1	17.1	10.3
dune buggy	64.6	45.4	50.2	33.9	22.7	14.5
egyptian cat	71.8	53.1	44.8	32.0	11.4	8.4
english springer	75.1	62.2	48.0	38.9	12.5	9.5
eskimo dog	90.7	67.3	66.6	45.0	22.4	15.7
eyeglasses	74.5	55.1	59.4	43.1	28.1	19.5
f1 car	77.4	54.3	58.0	37.7	22.8	14.4
fighter jet	67.8	55.0	54.1	44.8	21.6	18.4
fire truck	80.3	54.5	55.5	37.7	20.4	12.6
folding chair	85.3	44.6	71.7	37.9	35.4	19.1
forklift	79.5	48.2	62.0	34.8	26.4	13.9
french horn	62.8	34.9	40.5	19.0	7.9	3.7
garbage truck	82.0	65.0	66.4	48.6	28.8	20.5
gazelle	90.7	78.4	65.9	50.7	19.4	14.9
glider	78.4	66.6	64.6	54.5	31.4	27.0
go kart	77.0	58.0	52.8	40.5	18.6	12.0
golden retriever	81.9	63.4	56.5	42.3	21.2	16.1
gordon setter	82.6	68.9	57.6	44.4	17.3	13.5
guitar	91.2	79.8	79.3	49.5	35.6	18.1
hacksaw	69.3	56.5	53.6	43.3	19.8	16.3
hair dryer	67.1	55.4	47.8	37.8	16.0	12.6
hartebeest	85.1	77.0	60.9	50.6	16.4	12.1
highchair	74.7	41.5	51.4	27.2	16.5	7.9
ibex	84.9	70.6	54.8	42.2	15.7	12.0
ice bear	82.9	66.9	59.1	42.8	21.2	15.3
impala	89.9	69.1	63.8	46.7	21.4	15.1
irish water spaniel	83.6	71.0	56.7	49.3	18.0	17.3
iron	60.0	53.2	44.9	40.4	17.8	15.9
japanese spaniel	78.4	59.3	47.5	36.4	15.1	11.9
jinrikisha	72.2	44.4	54.6	31.8	22.2	12.6
kettle	68.6	49.5	38.7	27.8	9.8	7.3
kettle electric	71.9	67.5	46.4	41.9	15.9	14.1
knife	87.7	83.4	68.0	54.0	33.8	27.7
leopard	86.2	73.1	64.7	50.8	23.2	17.8
megaphone	81.5	71.0	59.5	49.5	20.1	16.7
microwave	67.1	49.5	47.2	35.1	17.9	13.9
motor scooter	72.1	65.6	51.9	47.0	22.7	20.1
motorbike	72.9	74.2	56.7	59.2	26.7	28.3
office chair	77.0	44.8	55.5	33.3	20.0	12.1
ox	78.1	62.4	47.5	35.1	12.7	8.8
pickup truck	87.0	47.8	74.1	39.7	37.0	20.2
power drill	75.9	66.0	47.6	41.4	13.6	12.7
ram	82.0	65.0	50.1	36.2	15.2	10.0
redbone	90.2	70.4	71.9	53.4	26.1	19.3
rifle	75.2	70.9	64.4	59.6	32.4	30.3
saint bernard	89.5	72.7	61.7	46.7	18.0	13.8
saluki	85.4	76.1	67.5	54.7	25.6	20.4
saxophone	72.9	63.2	50.3	39.3	19.2	14.4

Continued on next page

Category	PCK@0.10		PCK@0.05		PCK@0.02	
	CC	SOC	CC	SOC	CC	SOC
school bus	85.7	53.5	72.7	43.8	36.5	21.1
segway	67.2	46.3	38.8	26.1	12.6	7.8
sewing machine	76.3	71.1	59.5	55.0	25.7	24.3
sloth bear	69.3	52.0	37.0	26.9	8.5	6.3
snowmobile	74.7	64.4	54.6	45.4	22.9	18.1
sofa	76.9	52.8	56.6	39.7	22.2	16.4
soft coated wheaten terrier	79.0	60.5	41.9	31.5	12.2	9.9
sorrel	75.6	55.8	44.6	30.1	9.9	6.5
sports car	90.6	64.7	73.4	47.0	28.9	18.4
tank	67.5	56.8	51.4	43.5	19.7	16.0
teapot	74.8	69.0	47.6	45.0	18.6	18.0
tibetan terrier	68.4	57.6	40.9	33.9	10.6	8.7
tiger	88.8	69.9	68.2	51.4	25.0	19.5
timber wolf	88.4	72.6	62.2	48.9	20.6	16.2
tractor	86.7	61.3	64.7	43.4	23.0	16.3
train	75.8	51.2	52.6	35.2	21.0	13.5
tricycle	71.3	54.2	48.8	36.2	17.9	13.2
trolleybus	82.6	60.6	71.4	46.2	37.3	22.0
unicycle	57.7	58.3	29.1	29.6	7.4	8.0
violin	75.2	50.3	52.3	26.7	19.0	9.1
vizsla	89.1	72.4	73.9	58.3	30.0	23.5
walker hound	89.1	71.8	69.8	52.7	27.2	21.0
warthog	77.6	61.3	45.2	34.1	12.8	9.5
washer	75.0	60.6	61.0	48.1	25.9	19.5
water buffalo	73.2	54.8	37.8	27.0	8.8	6.3
weimaraner	88.6	69.7	65.6	49.9	23.2	18.3
wheelchair	78.4	43.1	61.3	33.6	24.5	13.4
zebra	91.3	75.1	66.0	47.2	17.9	13.1

B Example Annotations

We show example annotations in Fig. r2, illustrating the diversity of the selected categories. Further, it illustrates keypoints that are unique (red color) and keypoints that are shared across categories or correspond to the same semantic concept.

B.1 Limitations of Existing SC Annotations

Figure r3 shows concrete failure cases of keypoint annotations in existing SC benchmarks, illustrating the limitations summarized in Sec. 3.1 of the main paper: lack of semantic grounding, intra-class ambiguity, symmetry-induced non-uniqueness, and inconsistent definitions across instances.

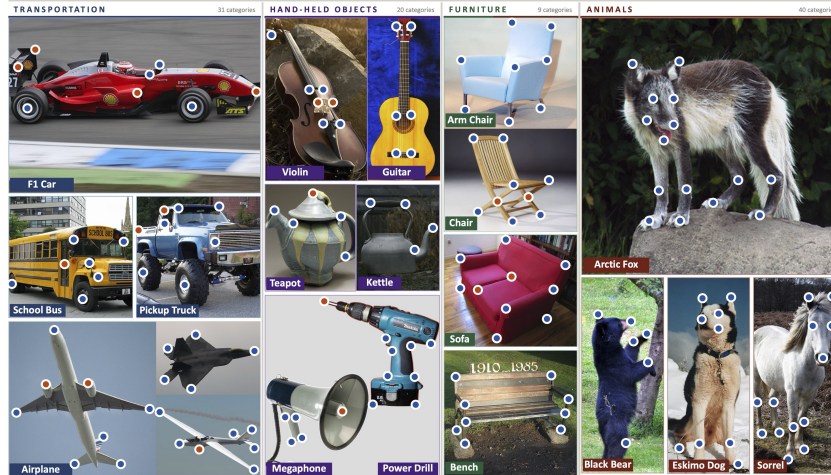


Fig. r2: Example SOCO annotations. We visualize example SOCO annotations where a red corresponds to a unique keypoint and blue to a shared keypoint.

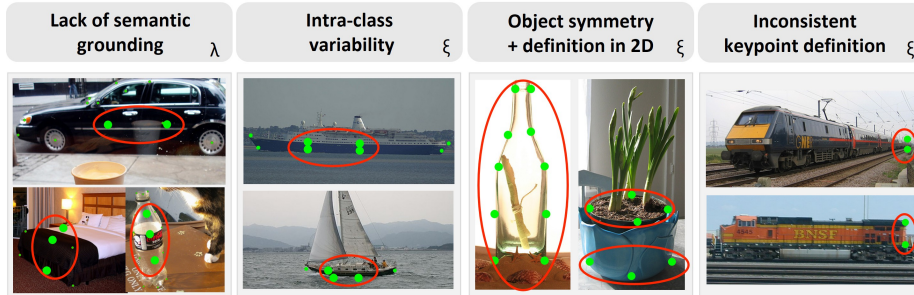


Fig. r3: Limitations of SC keypoint annotations. Current SC datasets include keypoints that lack semantic grounding and are mainly defined geometrically. This results in particularly ambiguous keypoint definitions for categories with large intra-class variability, e.g., boats. Uniqueness is not satisfied for symmetric objects where the keypoints are defined via a 2D projection (e.g., for *potted plant* and *bottle*). Furthermore, some keypoint definitions are inconsistent, for example for *trains*. Example images are sourced from MISC210K (λ) and SPair-71k (ξ).

C Evaluation Results for Other Tasks

C.1 Previous SC datasets

We report evaluation results for other SC datasets in Tab. r7. While the rankings for the best models and the worse models remain largely consistent and DINOv2 remains the best-performing model across all datasets, some model rankings change. For example, I-JEPA is ranked better for SOCO than for MISC or SPair. One potential explanation for this could be that I-JEPA is trained on ImageNet and SOCO images are also sourced from ImageNet. On the other hand, PE-Spatial’s relative performance drops on SOCO compared to, e.g., SPair. It is relevant to note that rankings for AP-10K and the SOCO animal subset are largely consistent, as both capture animal keypoint datasets. However, rankings change for the whole SOCO dataset, as man-made objects are added.

Table r7: Evaluation on other SC benchmarks. We report model PCK@0.1 performance with our standard evaluation protocol for MISC210K, SPair-71k, and, AP-10K. MISC* indicates that we only evaluate the single-instance correspondences, as this is the comparable setting. While DINOv2 remains the best model, other model rankings vary.

Model	MISC*	SPair	AP-10K
DINOv1	40.05	27.01	31.87
DINOv2	74.86	58.42	61.30
DINOv3	69.71	53.44	58.57
iBOT	50.63	34.95	44.14
I-JEPA	47.77	41.01	47.71
C-RADIOv3	70.56	49.05	51.45
DUNE	57.51	42.34	47.11
SD 2.1	60.15	45.95	45.33
CroCov2	16.01	8.41	10.00
MAE	13.46	6.62	10.08
PIXIO	52.39	37.50	39.28
CLIP	28.30	15.44	19.58
PE-Spatial	64.52	46.12	42.31
QWEN-L	34.69	16.40	16.74

C.2 Other Downstream Tasks

We report the correlation coefficients and confidence intervals of ImageNet kNN classification / SOC and other tasks in Tab. r9. Further, we report all results of selected models and datasets in Table r8 and visualize them in Fig. r4.

Table r8: Performance on various downstream tasks. We present the results for various tasks and models, as presented in the main paper.

model	ImageNet	SemSeg	3D Det.	3D-Pose	MV Corr.	Tracking	Normals	Depth
	kNN top-1 \uparrow	ADE20K mIoU \uparrow	ARKit AP3D \uparrow	ImageNet3D err $< \pi/6$ \uparrow	NAVI PCK θ_{30}^{60} \uparrow	TAP-Vid-D. AJ \uparrow	NYUv2 RMSE \downarrow	NYUv2 RMSE \downarrow
DINov1	74.87	0.23	28.97	0.42	56.15	19.48	30.24	0.43
DINov2	81.59	0.44	45.37	0.53	70.68	22.86	23.31	0.26
DINov3	82.43	0.34	46.70	0.53	76.80	22.07	24.09	0.27
iBOT	76.47	0.28	32.96	0.41	58.40	19.71	29.33	0.40
I-JEPA	60.62	0.16	41.45	0.53	55.74	17.55	24.67	0.27
C-RADIOv3	76.98	0.47	46.70	0.45	67.69	19.41	24.57	0.28
DUNE	56.21	0.32	43.10	0.42	65.74	24.75	23.65	0.27
SD 2.1	10.37	0.27	30.27	0.37	63.32	18.94	25.88	0.34
CroCov2	18.03	0.13	26.53	0.39	44.36	14.29	29.13	0.41
MAE	46.75	0.14	20.60	0.42	40.05	13.36	51.93	0.55
PIXIO	58.18	0.39	39.63	0.55	64.18	17.72	24.68	0.23
CLIP	71.44	0.18	27.93	0.36	36.29	12.51	31.00	0.40
PE-Spatial	51.11	0.42	40.63	0.37	60.99	20.24	28.22	0.32

Table r9: Correlation coefficients for downstream tasks. Pearson correlation coefficients with 95% confidence intervals between downstream-task performance and SOCO / ImageNet kNN. The results correspond to the bar plot in the main paper.

Task	SOCO		kNN	
	r	95% CI	r	95% CI
Seg.	0.629	[0.422, 0.795]	0.399	[0.121, 0.646]
Det3	0.892	[0.801, 0.949]	0.393	[0.027, 0.631]
Pose	0.692	[0.528, 0.823]	0.348	[0.071, 0.566]
MV Corr.	0.943	[0.912, 0.969]	0.266	[-0.087, 0.562]
Tracking	0.907	[0.844, 0.956]	0.286	[-0.106, 0.594]
Normals	-0.737	[-0.867, -0.673]	-0.395	[-0.698, -0.084]
Depth	-0.798	[-0.888, -0.668]	-0.298	[-0.570, -0.069]

D More Details on the Performed Evaluations

D.1 Details on SOC Evaluation

We follow the evaluation protocol in Probe3D [20] for all semantic correspondence evaluations. Specifically, we compute PCK@0.1 with bounding box normalization and the per-category PCK using the *per-keypoint* convention, as also applied in other recent works, e.g., [79]. The final result is computed using the average over categories and we keep a fixed image resolution of 800 pixels.

D.2 Details on Evaluated Models

We evaluate a diverse set of visual backbones spanning self-supervised, vision-language, generative, and 3D-aware training regimes, as summarized in Table r10. All backbones are kept frozen throughout our experiments. Zero-shot settings operate directly on the backbone features without any learnable components, while probed settings attach lightweight task-specific heads (e.g., linear or DPT-style decoders) trained on top of the fixed representations. This design

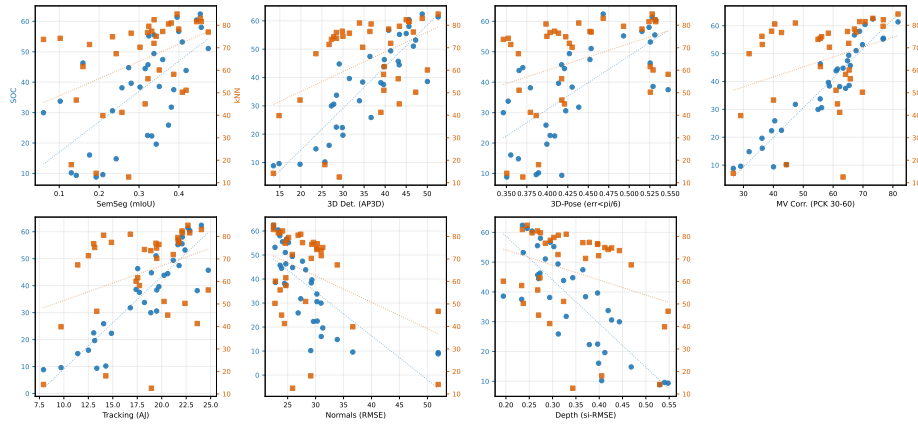


Fig. r4: SOC and kNN performance vs. downstream task performance. We plot the model performances for the compared models (as reported in Tab. r8).

ensures that downstream performance reflects differences in representation quality rather than task-specific fine-tuning capacity.

D.3 Details on Other Downstream Tasks

We extend Probe3D [20], a 3D-awareness evaluation framework into a broader, unified evaluation suite spanning monocular geometry, multi-view correspondence, semantic segmentation, tracking, classification, and 3D detection. This section details the tasks, datasets, probe architectures, and evaluation protocols used, as well as the backbone families we evaluate.

The extended suite covers the following task families:

Correspondence (zero-shot). We evaluate correspondence in two regimes: **semantic matching** and **multiview geometric matching**. For SPair-71k [45], we follow Probe3D [20] and extract feature vectors at annotated keypoints, predicting matches via nearest-neighbor similarity and reporting PCK@0.1. For NAVI [31], we extract feature maps for both views and establish correspondences using nearest-neighbor matching in feature space, followed by Lowe’s ratio test to retain reliable matches. Candidate correspondences are triangulated using ground-truth camera calibration, and accuracy is measured as the fraction of matches whose 3D error is below 2 cm. Following the Probe3D protocol, we stratify the 2 cm recall by relative camera rotation and report performance in the hardest bin, corresponding to pairs with viewpoint change in the $[90^\circ, 120^\circ)$ range.

ImageNet classification (kNN). We perform ImageNet classification using k -nearest neighbors. For this embeddings are extracted on the ImageNet training set and evaluated on the validation set. We select the k -value that results in

Table r10: Evaluated visual models. We list architecture, supervision type, and pre-training data for the evaluated backbones presented in the main paper. Whenever possible, we use publicly released checkpoints of comparable scale.

Model	Architecture	Supervision	Pre-train data
DINOv1 [13]	ViT-B/16	SSL	ImageNet-1K
DINOv2 [47]	ViT-B/14	SSL	LVD-142M
DINOv3 [60]	ViT-B/16	SSL	LVD-1689M
iBOT [82]	ViT-B/16	SSL	ImageNet-1K
I-JEPA [3]	ViT-H/16	SSL (JEPA)	ImageNet-1K
C-RADIOv3 [29]	ViT-H/16	Distill.	NV-CC-T2I-Dataset 700M
DUNE [54]	ViT-B/14	Distill.	DUNE-20.7M
SD 2.1 [53]	U-Net	T2I gen.	LAION-5B
CroCov2 [70]	ViT-B/16	MV SSL	HM3D, ScanNet, etc.
MAE [28]	ViT-B/16	SSL (MIM)	ImageNet-1K
PIXIO [76]	ViT-B/16	SSL (MIM)	Curated MetaCLIP-2B
CLIP [48]	ViT-B/16	Contrastive	~400M image-text pairs
PE-Spatial [9]	ViT-G/14	Contrastive	Curated 5.4B MetaCLIP pairs
Qwen2.5-VL [7]	ViT-H	VLM	4T token multimodal data

the best classification accuracy. Following common practice, classification is performed using the CLS token if available. Otherwise, dense tokens are averaged into one vector.

Semantic segmentation (probed). Dense semantic understanding is assessed on ADE20K [81] using a minimal segmentation probe. We train a lightweight linear segmentation head consisting of a single 1×1 convolution applied to dense frozen backbone features on ADE20K. The probe is trained for 25 epochs using SGD, and we report mean IoU on the validation set.

Tracking (zero-shot). We assess spatio-temporal consistency via zero-shot point tracking on TAP-Vid-DAVIS [17]. Dense feature maps are extracted for each frame, and query points are embedded by bilinear sampling in feature space at their first visible location. For each subsequent frame, we compute the cosine similarities between the query descriptor and the dense feature map, and obtain correspondences via argmax operation. Evaluation follows the TAP-Vid queried-first protocol, and we report Average Jaccard (AJ) [4], which jointly captures occlusion consistency and point localization accuracy.

Monocular geometry (probed). We evaluate single-image geometric prediction on NYUv2 [59] using two tasks: depth estimation and surface normal prediction. Following the Probe3D [20] setup, we attach a lightweight DPT-style multiscale decoder to frozen backbone features extracted from several intermediate blocks. For depth estimation, we use metric depth on NYUv2 and evaluate performance using the root mean squared error (RMSE) between predicted and ground-truth depth maps. For surface normals, the decoder predicts per-pixel normal directions, and accuracy is assessed using the RMSE of angular errors between predicted and ground-truth normals, providing a direct measure of local geometric fidelity.

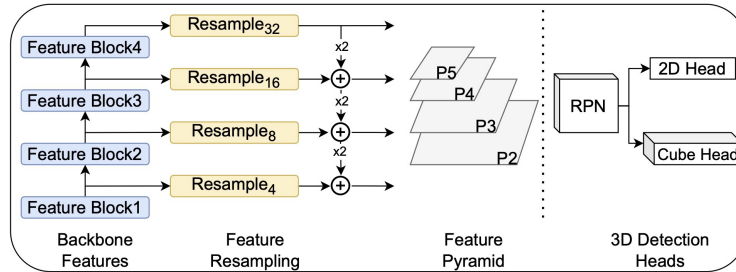


Fig. r5: Overview of the detection probe. The probe receives four intermediate feature maps from a pretrained frozen backbone, merges and upsamples them to produce a Detectron2-style feature pyramid $\{p_2, p_3, p_4, p_5\}$ used by the 3D detection head.

3D pose estimation (probed). We evaluate object-level 3D awareness on ImageNet3D [41] by linearly probing frozen backbone features for 3D viewpoint prediction. Following the ImageNet3D protocol, three independent linear probes are trained to predict azimuth, elevation, and in-plane rotation from pooled backbone features. The predicted angle distributions are converted to continuous rotation matrices, and performance is measured using the geodesic rotation error [41], defined as the angle of the matrix logarithm of $R_{\text{pred}}^\top R_{\text{gt}}$. We report pose accuracy as the percentage of samples whose rotation error is below a threshold of $\pi/6$.

3D detection (probed). Our experiments build on the Omni3D [10] detection pipeline, which extends Detectron2 [72] with Cube R-CNN style 3D cuboid prediction. While the original setup optimizes a CNN backbone, we repurpose it as a 3D detection head on top of frozen, pretrained visual encoders (eg., DINO/v2/v3, CLIP, SD etc.). To bridge the gap between pre-trained backbones and 3D detection heads, we introduce a lightweight DPT [49] probe, and the resulting features are reassembled to form a feature pyramid (see Figure r5). Given a pretrained backbone, we select four feature blocks at increasing depth and reshape their patch tokens into dense spatial feature maps. These maps all share the same spatial resolution (the patch grid) but capture progressively higher-level semantics. The four features are fed into the probe, which first unifies channel dimensions with 1×1 convolutions, then constructs a top-down FPN [35] style decoder. Through resampling and lateral fusion, the probe produces a Detectron2-compatible feature pyramid.

We attach the probe and detection heads to frozen backbone features and train on a subset of indoor RGB-D scenes with 3D bounding box annotations. We report average precision (AP3D) for ARKitScenes [8] subset of Omni3D in Table r8.

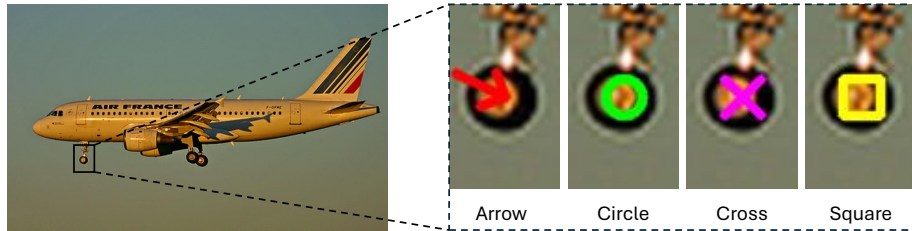


Fig. r6: Examples of visual markers to indicate keypoints for LVLM evaluation.

Table r11: Evaluation of visual prompts. Average performance of Qwen2.5-VL-7B-Instruct given different visual prompts.

Marker shape	Mean	Marker color	Mean
Arrow	30.0	Red	30.0
Circle	29.8	Blue	29.3
Cross	28.0	Yellow	28.9
Square	26.6	Purple	28.2
		Green	27.4

D.4 More Details of LVLM Evaluation

Implementation details. We use the VLMEvalKit [39] framework to perform standardized evaluation across different LVLMs. For the evaluation, we pursue a similar setup as [24]. GPT-4o is employed as a judge to verify whether an LVLM’s output matches the ground-truth answer. From the annotated SOCO data, we construct 2,000 multiple-choice questions. For each question, we provide the human-annotated semantically matched keypoint as the ground-truth answer and use other randomly sampled annotated keypoints in the target image as distractor options.

Prompts: We illustrate the evaluation setting and present prompt examples for the LVLM evaluation under different settings in Fig. r7a, Fig. r7c, and Fig. r7b. For the *Vis.* setting, we provide BLINK-style questions with the red arrow marker in the source image. For *Vis.+Desc.*, we additionally include a templated keypoint description alongside the visual marker. For the *Desc.* setting, the source image is omitted and the query keypoint is specified only through its textual description; the target image with candidate markers remains visible.

Choices of visual markers: The BLINK benchmark uses a red circle to mark keypoints for LVLMs to attend to. Previous work [12,58] has shown that different visual markers can affect VLM performance. Here, we investigate alternative visual markers for keypoints to study their impact. We experiment with different colors and shapes of visual markers, with examples shown in Figure r6.

To assess how robust LVLMs are to different visual markers, we follow the BLINK benchmark and build a smaller benchmark of SPair-71k to search for markers that yield the highest accuracy. Following the BLINK protocol, we

construct 233 questions and we present results using Qwen2.5-VL-7B-Instruct across all settings. Table r11 reports the average performance of the LVLM under different marker shapes and colors. We observe that the arrow shape and red color achieve the best performance among the tested options respectively. Consequently, we assume this setting also generalizes to the SOCO dataset and we adopt red arrow as the default visual marker in all LVLM experiments.

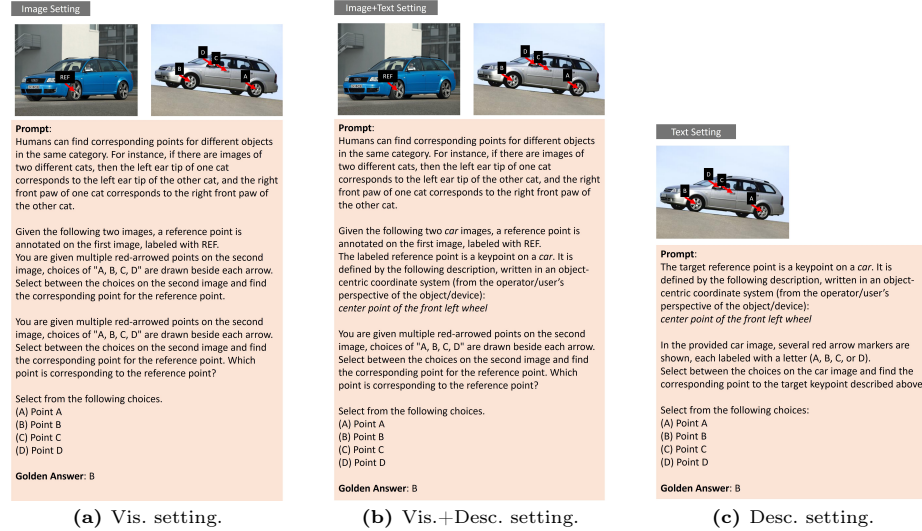


Fig. r7: Example prompts for LVLM evaluation in the three settings *image*, *image+text*, and *text*.

E More Details about Annotation Pipeline

Figure r8 presents an example GUI that was shown to the AMT workers that were hired for labeling the keypoints. Reference annotations were given on representative images for each keypoint. Every AMT worker had to pass a qualification test before annotating and continuous monitoring ensured sufficient labeling quality.

F Limitations

Sparse keypoint annotations. SOCO provides characteristic part correspondences via sparse keypoint labels rather than dense semantic matching. This is sufficient for diagnosing structured part-level understanding, but it does not support evaluating dense pixel-wise correspondence *per-se*.

Image-source bias. Images are sourced from ImageNet3D [41] and Animal3D [74], which enables inherited 3D pose metadata and in-distribution evaluation of ImageNet-trained models but biases the dataset toward salient, curated object views and limits the evaluation of out-of-distribution scenarios.

Prompted LVLMM setting. Keypoint descriptions are template-based. More detailed natural language descriptions could improve the LVLMM performance further.

Zero-shot nearest-neighbor matching. SOC is mainly designed as a zero-shot diagnostic. Therefore, the default vision-model evaluation uses nearest-neighbor feature matching, which is intentionally simple and forms a lower bound on what a given representation can support with supervised adaptation.

Cross-category taxonomy scope. Cross-category correspondences are defined within the proposed concept hierarchy. Broader functional analogies that fall outside this hierarchy (e.g. tool affordance transfer across distant categories) remain future work.

G Ethical Concerns

The SOCO dataset includes a small number of images depicting military equipment (specifically the categories *tank*, *rifle*, and *fighter jet*), but these objects are shown in non-violent contexts and do not directly capture physical harm. All images were sourced from public datasets [16, 41]. The purpose of the dataset is exclusively methodological: to study semantic correspondence and representation learning for diverse categories. Nonetheless, we acknowledge that models could be evaluated on data containing weapons in principle and could be potentially applied in harmful downstream applications.

Instructions (click to hide/show)

Please read the instructions when you perform this task for the first time. We automatically check assignments and we need to reject the ones that do not satisfy the basic requirements as explained below. When you are rejected, you will receive a Bonus (50% additional payment). If annotations are not accurate, we will revoke the qualification.

Task: All keypoints need to be labeled. A marked keypoint (with left mouse click (if visible) or with X with button ⌘ (if not visible))

- For the currently selected keypoint, the reference image shows the annotation on an example image of the given object category.
- Label the keypoint at the corresponding location as accurate as possible, but only if the so-labeled keypoint is completely visible.
- Mark the center point of a specified object part if it is not specified differently.
- Mark the center point of a specified object part if it is not specified differently and not the background (for example, the center point of a wheel).
- Click the submit button (bottom right corner) once all keypoints have been annotated (or marked invisible).

Annotation procedure: Click the left mouse button to place a keypoint. Zoom in for more accurate labeling. You can drag the point to adjust its position.

Invisible or ambiguous keypoints: If the point is not clearly visible, press **h** or click the eye symbol to mark it as invisible (i). Do not set keypoints at arbitrary places if they cannot be clearly identified or are ambiguous.

Conventions: Left vs. right / front vs. back / top vs. bottom are defined in the object coordinate system. Ensure that you understand how the orientation and the front side of an object are defined. Two examples are on the right: 1) Left hand means left hand from the driver's perspective. 2) The chair is pointing towards the observer. Therefore, the keypoints on the chair's right side are on the left in the image.

Conventions

Instructions | **Shortcuts**

Canvas Coordinates: (825, 457) Image Coordinates: (591, 439)

Object: 1: bicycle

Keypoint Classes

- 1: bike_frame_left_center
- 2: bike_frame_right_center
- 3: bike_seat_center
- 4: bike_pedal_center
- 5: bike_wheel_center
- 6: bike_handlebar_center
- 7: bike_headlight_center
- 8: bike_rearview_mirror_center
- 9: bike_bell_center
- 10: bike_bell_center
- 11: bike_rearview_mirror_center
- 12: handlebar_left_center
- 13: handlebar_right_center

Reference image

Use this reference image to guide your keypoint annotations on the right.

Submit

Fig. r8: Example AMT labeling GUI. This GUI was presented to Amazon Mechanical Turk workers for keypoint labeling.

References

1. Alayrac, J.B., Donahue, J., Luc, P., Miech, A., Barr, I., Hasson, Y., Lenc, K., Mensch, A., Millicah, K., Reynolds, M., Ring, R., Rutherford, E., Cabi, S., Han, T., Gong, Z., Samangooei, S., Monteiro, M., Menick, J., Borgeaud, S., Brock, A., Nematzadeh, A., Sharifzadeh, S., Binkowski, M., Barreira, R., Vinyals, O., Zisserman, A., Simonyan, K.: Flamingo: A visual language model for few-shot learning. *NeurIPS* **35** (2022)
2. Andriluka, M., Pishchulin, L., Gehler, P., Schiele, B.: 2D human pose estimation: New benchmark and state of the art analysis. In: *CVPR*. pp. 3686–3693 (2014)
3. Assran, M., Duval, Q., Misra, I., Bojanowski, P., Vincent, P., Rabbat, M., Lecun, Y., Ballas, N.: Self-supervised learning from images with a joint-embedding predictive architecture. In: *CVPR*. pp. 15619–15629 (2023)
4. Aydemir, G., Xie, W., Güney, F.: Can visual foundation models achieve long-term point tracking? In: *ECCV Workshops* (2024)
5. Bai, J., Bai, S., Yang, S., Wang, S., Tan, S., Wang, P., Lin, J., Zhou, C., Zhou, J.: Qwen-VL: A versatile vision-language model for understanding, localization, text reading, and beyond. *arXiv preprint arXiv:2308.12966* (2023)
6. Bai, S., Cai, Y., Chen, R., Chen, K., Chen, X., Cheng, Z., Deng, L., Ding, W., Gao, C., Ge, C., et al.: Qwen3-VL technical report. *arXiv preprint arXiv:2511.21631* (2025)
7. Bai, S., Chen, K., Liu, X., Wang, J., Ge, W., Song, S., Dang, K., Wang, P., Wang, S., Tang, J., Zhong, H., Zhu, Y., Yang, M., Li, Z., Wan, J., Wang, P., Ding, W., Fu, Z., Xu, Y., Ye, J., Zhang, X., Xie, T., Cheng, Z., Zhang, H., Yang, Z., Xu, H., Lin, J.: Qwen2.5-VL technical report. *arXiv preprint arXiv:2502.13923* (2025)
8. Baruch, G., Chen, Z., Dehghan, A., Dimry, T., Feigin, Y., Fu, P., Gebauer, T., Joffe, B., Kurz, D., Schwartz, A., Shulman, E.: ARKitScenes: A diverse real-world dataset for 3D indoor scene understanding using mobile RGB-D data. *arXiv preprint arXiv:2111.08897* (2021)
9. Bolya, D., Huang, P.Y., Sun, P., Cho, J.H., Madotto, A., Wei, C., Ma, T., Zhi, J., Rajasegaran, J., Rasheed, H., et al.: Perception encoder: The best visual embeddings are not at the output of the network. *arXiv preprint arXiv:2504.13181* (2025)
10. Brazil, G., Kumar, A., Straub, J., Ravi, N., Johnson, J., Gkioxari, G.: Omni3D: A large benchmark and model for 3D object detection in the wild. In: *CVPR* (2023)
11. Butler, D.J., Wulff, J., Stanley, G.B., Black, M.J.: A naturalistic open source movie for optical flow evaluation. In: *ECCV*. pp. 611–625 (2012)
12. Cai, Z., Yeh, C.F., Xu, H., Liu, Z., Meyer, G., Lei, X., Zhao, C., Li, S.W., Chandra, V., Shi, Y.: DepthLM: Metric depth from vision language models. *arXiv preprint arXiv:2509.25413* (2025)
13. Caron, M., Touvron, H., Misra, I., Jégou, H., Mairal, J., Bojanowski, P., Joulin, A.: Emerging properties in self-supervised vision transformers. In: *ICCV* (2021)
14. Chi, Y., Sommer, L., Dünkel, O., Muhle, D., Cremers, D., Theobalt, C., Kortylewski, A.: C3PO: Canonicalization of 3D pose from partial views with generalizable correspondence features. In: *3DV* (2026)
15. Cordts, M., Omran, M., Ramos, S., Rehfeld, T., Enzweiler, M., Benenson, R., Franke, U., Roth, S., Schiele, B.: The cityscapes dataset for semantic urban scene understanding. In: *CVPR*. pp. 3213–3223 (2016)
16. Deng, J., Dong, W., Socher, R., Li, L.J., Li, K., Fei-Fei, L.: ImageNet: A large-scale hierarchical image database. In: *CVPR*. pp. 248–255 (2009)

17. Doersch, C., Gupta, A., Markeeva, L., Recasens, A., Smaira, L., Aytar, Y., Carreira, J., Zisserman, A., Yang, Y.: TAP-Vid: A benchmark for tracking any point in a video. *NeurIPS* **35**, 13610–13626 (2022)
18. Dünkel, O., Jesslen, A., Xie, J., Theobalt, C., Rupperecht, C., Kortylewski, A.: CNS-Bench: Benchmarking image classifier robustness under continuous nuisance shifts. In: *ICCV* (2025)
19. Dünkel, O., Wimmer, T., Theobalt, C., Rupperecht, C., Kortylewski, A.: Do it yourself: Learning semantic correspondence from pseudo-labels. In: *ICCV* (2025)
20. El Banani, M., Raj, A., Maninis, K.K., Kar, A., Li, Y., Rubinstein, M., Sun, D., Guibas, L., Johnson, J., Jampani, V.: Probing the 3D awareness of visual foundation models. In: *CVPR*. pp. 21795–21806 (2024)
21. Everingham, M., Eslami, S.M.A., Van Gool, L., Williams, C.K.I., Winn, J., Zisserman, A.: The PASCAL visual object classes challenge: A retrospective. *IJCV* **111**(1), 98–136 (2015)
22. Everingham, M., Van Gool, L., Williams, C.K.I., Winn, J., Zisserman, A.: The PASCAL visual object classes (VOC) challenge. *IJCV* **88**(2), 303–338 (2010)
23. Florence, P.R., Manuelli, L., Tedrake, R.: Dense object nets: Learning dense visual object descriptors by and for robotic manipulation. *arXiv preprint arXiv:1806.08756* (2018)
24. Fu, X., Hu, Y., Li, B., Feng, Y., Wang, H., Lin, X., Roth, D., Smith, N.A., Ma, W.C., Krishna, R.: BLINK: Multimodal large language models can see but not perceive. In: *ECCV* (2024)
25. Gan, C., Tu, Y., Chen, X., Chen, T., Li, Y., Harandi, M., Lin, W.: Unleashing diffusion transformers for visual correspondence by modulating massive activations. In: *NeurIPS* (2025)
26. Gemini Team: Gemini: A family of highly capable multimodal models. *arXiv preprint arXiv:2312.11805* (2023)
27. Ham, B., Cho, M., Schmid, C., Ponce, J.: Proposal flow. In: *CVPR*. pp. 3475–3484 (2016)
28. He, K., Chen, X., Xie, S., Li, Y., Dollár, P., Girshick, R.: Masked autoencoders are scalable vision learners. In: *CVPR*. pp. 16000–16009 (2022)
29. Heinrich, G., Ranzinger, M., Yin, H., Lu, Y., Kautz, J., Tao, A., Catanzaro, B., Molchanov, P.: RADIOv2.5: Improved baselines for agglomerative vision foundation models. In: *CVPR* (2025)
30. Hurst, A., Lerer, A., Goucher, A.P., Perelman, A., Ramesh, A., Clark, A., Ostrow, A.J., Welihinda, A., Hayes, A., Radford, A., et al.: GPT-4o system card. *arXiv preprint arXiv:2410.21276* (2024)
31. Jampani, V., Maninis, K.K., Engelhardt, A., Karpur, A., Truong, K., Sargent, K., Popov, S., Araujo, A., Martin-Brualla, R., Patel, K., Vlasic, D., Ferrari, V., Makadia, A., Liu, C., Li, Y., Zhou, H.: NAVI: Category-agnostic image collections with high-quality 3D shape and pose annotations. In: *NeurIPS* (2023)
32. Kornblith, S., Shlens, J., Le, Q.V.: Do better ImageNet models transfer better? In: *CVPR*. pp. 2661–2671 (2019)
33. Li, B., Zhang, Y., Guo, D., Zhang, R., Li, F., Zhang, H., Zhang, K., Zhang, P., Li, Y., Liu, Z., Li, C.: LLaVA-OneVision: Easy visual task transfer. *TMLR* (2024)
34. Li, J., Li, D., Xiong, C., Hoi, S.: BLIP: Bootstrapping language-image pre-training for unified vision-language understanding and generation. In: *ICML* (2022)
35. Lin, T.Y., Dollár, P., Girshick, R., He, K., Hariharan, B., Belongie, S.: Feature pyramid networks for object detection. In: *CVPR*. pp. 936–944 (2017)

36. Lin, T.Y., Maire, M., Belongie, S., Hays, J., Perona, P., Ramanan, D., Dollár, P., Zitnick, C.L.: Microsoft COCO: Common objects in context. In: ECCV. pp. 740–755 (2014)
37. Liu, C., Yuen, J., Torralba, A., Sivic, J., Freeman, W.T.: SIFT flow: Dense correspondence across different scenes. In: ECCV. pp. 28–42 (2008)
38. Liu, H., Li, C., Wu, Q., Lee, Y.J.: Visual instruction tuning. In: NeurIPS (2023)
39. Liu, Y., Duan, H., Zhang, Y., Li, B., Zhang, S., Zhao, W., Yuan, Y., Wang, J., He, C., Liu, Z., et al.: MMBench: Is your multi-modal model an all-around player? In: ECCV. pp. 216–233 (2024)
40. Luo, G., Dunlap, L., Park, D.H., Holynski, A., Darrell, T.: Diffusion hyperfeatures: Searching through time and space for semantic correspondence. In: NeurIPS (2023)
41. Ma, W., Zhang, G., Liu, Q., Zeng, G., Kortylewski, A., Liu, Y., Yuille, A.: ImageNet3D: Towards general-purpose object-level 3D understanding. NeurIPS **37**, 96127–96149 (2024)
42. Mariotti, O., Du, Z., Bhalgat, Y., Mac Aodha, O., Bilen, H.: Jamais vu: Exposing the generalization gap in supervised semantic correspondence. arXiv preprint arXiv:2506.08220 (2025)
43. Mariotti, O., Mac Aodha, O., Bilen, H.: Improving semantic correspondence with viewpoint-guided spherical maps. In: CVPR. pp. 19521–19530 (2024)
44. Mayer, N., Ilg, E., Haussler, P., Fischer, P., Cremers, D., Dosovitskiy, A., Brox, T.: A large dataset to train convolutional networks for disparity, optical flow, and scene flow estimation. In: CVPR. pp. 4040–4048 (2016)
45. Min, J., Lee, J., Ponce, J., Cho, M.: SPair-71k: A large-scale benchmark for semantic correspondence. arXiv preprint arXiv:1908.10543 (2019)
46. OpenAI, Applin, S., Adesso, G., Ashfaq, R., Bai, M., Brammer, M., Fecht, E., Goodman, A., Grossman, S., Groh, M., Kirk, H.R., Gunitsky, S., Huang, Y., Kahn, L., Kumar, S., Madrid-Morales, D., Motoki, F., Ovadya, A., Peters, U., Robinson, M., Röttger, P., Wasserman, H., Wehsener, A., Walker, L., Vidgen, B., Zhu, J.: GPT-4V(ision) system card. Tech. rep., OpenAI (2023)
47. Oquab, M., Darcet, T., Moutakanni, T., Vo, H.V., Szafraniec, M., Khalidov, V., Fernandez, P., Haziza, D., Massa, F., El-Nouby, A., Howes, R., Huang, P.Y., Xu, H., Sharma, V., Li, S.W., Galuba, W., Rabbat, M., Assran, M., Ballas, N., Synnaeve, G., Misra, I., Jégou, H., Mairal, J., Labatut, P., Joulin, A., Bojanowski, P.: DINOv2: Learning robust visual features without supervision. TMLR (2024)
48. Radford, A., Kim, J.W., Hallacy, C., Ramesh, A., Goh, G., Agarwal, S., Sastry, G., Askell, A., Mishkin, P., Clark, J., et al.: Learning transferable visual models from natural language supervision. In: ICML. pp. 8748–8763 (2021)
49. Ranftl, R., Bochkovskiy, A., Koltun, V.: Vision transformers for dense prediction. In: ICCV. pp. 12179–12188 (2021)
50. Ranzinger, M., Heinrich, G., Kautz, J., Molchanov, P.: AM-RADIO: Agglomerative vision foundation model reduce all domains into one. In: CVPR. pp. 12490–12500 (2024)
51. Ranzinger, M., Heinrich, G., McCarthy, C., Kautz, J., Tao, A., Catanzaro, B., Molchanov, P.: C-RADIOv4 technical report. arXiv preprint arXiv:2601.17237 (2026)
52. Rocco, I., Arandjelovic, R., Sivic, J.: Convolutional neural network architecture for geometric matching. In: CVPR. pp. 6148–6157 (2017)
53. Rombach, R., Blattmann, A., Lorenz, D., Esser, P., Ommer, B.: High-resolution image synthesis with latent diffusion models. In: CVPR. pp. 10684–10695 (2022)

54. Sariyıldız, M.B., Weinzaepfel, P., Lucas, T., De Jorge, P., Larlus, D., Kalantidis, Y.: DUNE: Distilling a universal encoder from heterogeneous 2D and 3D teachers. In: CVPR. pp. 30084–30094 (2025)
55. Scharstein, D., Szeliski, R.: A taxonomy and evaluation of dense two-frame stereo correspondence algorithms. *IJCV* **47**(1), 7–42 (2002)
56. Sedaghat, N., Brox, T.: Unsupervised generation of a viewpoint annotated car dataset from videos. In: ICCV (2015)
57. Shen, S., Li, L.H., Tan, H., Bansal, M., Rohrbach, A., Chang, K.W., Yao, Z., Keutzer, K.: How much can CLIP benefit vision-and-language tasks? In: ICLR (2022)
58. Shtedritski, A., Rupprecht, C., Vedaldi, A.: What does CLIP know about a red circle? visual prompt engineering for VLMs. In: ICCV (2023)
59. Silberman, N., Hoiem, D., Kohli, P., Fergus, R.: Indoor segmentation and support inference from RGB-D images. In: ECCV (2012)
60. Siméoni, O., Vo, H.V., Seitzer, M., Baldassarre, F., Oquab, M., Jose, C., Khalidov, V., Szafraniec, M., Yi, S., Ramamonjisoa, M., Massa, F., Haziza, D., Wehrstedt, L., Wang, J., Darcet, T., Moutakanni, T., Sentana, L., Roberts, C., Vedaldi, A., Tolan, J., Brandt, J., Couprie, C., Mairal, J., Jégou, H., Labatut, P., Bojanowski, P.: DINOv3. arXiv preprint arXiv:2508.10104 (2025)
61. Sommer, L., Dünkel, O., Theobalt, C., Kortylewski, A.: Common3D: Self-supervised learning of 3D morphable models for common objects in neural feature space. In: CVPR. pp. 6468–6479 (2025)
62. Stracke, N., Baumann, S.A., Bauer, K., Fundel, F., Ommer, B.: CleanDIFT: Diffusion features without noise. In: CVPR. pp. 117–127 (2025)
63. Sun, Y., Huang, Y., Guo, H., Zhao, Y., Wu, R., Yu, Y., Ge, W., Zhang, W.: MISC210K: A large-scale dataset for multi-instance semantic correspondence. In: CVPR. pp. 7121–7130 (2023)
64. Tang, L., Jia, M., Wang, Q., Phoo, C.P., Hariharan, B.: Emergent correspondence from image diffusion. *NeurIPS* **36**, 1363–1389 (2023)
65. Tanai, T., Sinha, S.N., Sato, Y.: Joint recovery of dense correspondence and cosegmentation in two images. In: CVPR. pp. 4246–4255 (2016)
66. Venkataramanan, S., Pariza, V., Salehi, M., Knobel, L., Gidaris, S., Ramzi, E., Bursuc, A., Asano, Y.M.: Franca: Nested matryoshka clustering for scalable visual representation learning. arXiv preprint arXiv:2507.14137 (2025)
67. Wandel, K., Wang, H.: SemAlign3D: Semantic correspondence between RGB images through aligning 3D object-class representations. In: CVPR (2025)
68. Wang, H., Sridhar, S., Huang, J., Valentin, J., Song, S., Guibas, L.J.: Normalized object coordinate space for category-level 6D object pose and size estimation. In: CVPR. pp. 2642–2651 (2019)
69. Wang, W., Gao, Z., Gu, L., Pu, H., Cui, L., Wei, X., Liu, Z., Jing, L., Ye, S., Shao, J., et al.: InternVL3.5: Advancing open-source multimodal models in versatility, reasoning, and efficiency. arXiv preprint arXiv:2508.18265 (2025)
70. Weinzaepfel, P., Lucas, T., Leroy, V., Cabon, Y., Arora, V., Brégier, R., Csurka, G., Antsfeld, L., Chidlovskii, B., Revaud, J.: CroCo v2: Improved cross-view completion pre-training for stereo matching and optical flow. In: ICCV (2023)
71. Wu, Y., Lim, J., Yang, M.H.: Online object tracking: A benchmark. In: CVPR. pp. 2411–2418 (2013)
72. Wu, Y., Kirillov, A., Massa, F., Lo, W.Y., Girshick, R.: Detectron2 (2019), software
73. Xiang, Y., Mottaghi, R., Savarese, S.: Beyond PASCAL: A benchmark for 3D object detection in the wild. In: WACV. pp. 75–82 (2014)

74. Xu, J., Zhang, Y., Peng, J., Ma, W., Jesslen, A., Ji, P., Hu, Q., Zhang, J., Liu, Q., Wang, J., et al.: Animal3D: A comprehensive dataset of 3D animal pose and shape. In: ICCV. pp. 9099–9109 (2023)
75. Yang, J., Yang, S., Gupta, A.W., Han, R., Fei-Fei, L., Xie, S.: Thinking in space: How multimodal large language models see, remember and recall spaces. arXiv preprint arXiv:2412.14171 (2024)
76. Yang, L., Li, S.W., Li, Y., Lei, X., Wang, D., Mohamed, A., Zhao, H., Xu, H.: In pursuit of pixel supervision for visual pre-training. arXiv preprint arXiv:2512.15715 (2025)
77. Yu, H., Xu, Y., Zhang, J., Zhao, W., Guan, Z., Tao, D.: AP-10K: A benchmark for animal pose estimation in the wild. arXiv preprint arXiv:2108.12617 (2021)
78. Yue, X., Ni, Y., Zhang, K., Zheng, T., Liu, R., Zhang, G., Stevens, S., Jiang, D., Ren, W., Sun, Y., Wei, C., Yu, B., Yuan, R., Sun, R., Yin, M., Zheng, B., Yang, Z., Liu, Y., Huang, W., Sun, H., Su, Y., Chen, W.: MMMU: A massive multi-discipline multimodal understanding and reasoning benchmark for expert AGI. In: CVPR (2024)
79. Zhang, J., Herrmann, C., Hur, J., Chen, E., Jampani, V., Sun, D., Yang, M.H.: Telling left from right: Identifying geometry-aware semantic correspondence. In: CVPR. pp. 3076–3085 (2024)
80. Zhang, J., Herrmann, C., Hur, J., Polania Cabrera, L., Jampani, V., Sun, D., Yang, M.H.: A tale of two features: Stable Diffusion complements DINO for zero-shot semantic correspondence. *NeurIPS* **36**, 45533–45547 (2023)
81. Zhou, B., Zhao, H., Puig, X., Fidler, S., Barriuso, A., Torralba, A.: Scene parsing through ADE20K dataset. In: CVPR. pp. 633–641 (2017)
82. Zhou, J., Wei, C., Wang, H., Shen, W., Xie, C., Yuille, A., Kong, T.: iBOT: Image BERT pre-training with online tokenizer. In: ICLR (2022)